Heavy element abundances in giant stars of the globular clusters M4 and M5[1]

David Yong

Research School of Astronomy and Astrophysics, Australian National University, Mount Stromlo Observatory, Cotter Road, Weston Creek, ACT 2611, Australia

yong@mso.anu.edu.au

Amanda I. Karakas

Research School of Astronomy and Astrophysics, Australian National University, Mount Stromlo Observatory, Cotter Road, Weston Creek, ACT 2611, Australia

akarakas@mso.anu.edu.au

David L. Lambert

The W. J. McDonald Observatory, University of Texas, Austin, TX 78712

dll@astro.as.utexas.edu

Alessandro Chieffi

Istituto Nazionale di Astrofisica - Istituto di Astrofisica Spaziale e Fisica Cosmica, Via Fosso del Cavaliere, I-00133, Roma, Italy

alessandro.chieffi@iasf-roma.inaf.it

Marco Limongi

Istituto Nazionale di Astrofisica - Osservatorio Astronomico di Roma, Via Frascati 33, I-00040, Roma, Italy

marco@oa-roma.inaf.it

ABSTRACT

[1]Based on observations made with the Magellan Clay Telescope at Las Campanas Observatory.

We present a comprehensive abundance analysis of 27 heavy elements in bright giant stars of the globular clusters M4 and M5 based on high resolution, high signal-to-noise ratio spectra obtained with the Magellan Clay Telescope. We confirm and expand upon previous results for these clusters by showing that (1) all elements heavier than, and including, Si have constant abundances within each cluster, (2) the elements from Ca to Ni have indistinguishable compositions in M4 and M5, (3) Si, Cu, Zn, and all *s*-process elements are approximately 0.3 dex overabundant in M4 relative to M5, and (4) the *r*-process elements Sm, Eu, Gd, and Th are slightly overabundant in M5 relative to M4. The cluster-to-cluster abundance differences for Cu and Zn are intriguing, especially in light of their uncertain nucleosynthetic origins. We confirm that stars other than Type Ia supernovae must produce significant amounts of Cu and Zn at or below the clusters' metallicities. If intermediate-mass AGB stars or massive stars are responsible for the Cu and Zn enhancements in M4, the similar [Rb/Zr] ratios and (preliminary) Mg isotope ratios in both clusters may be problematic for either scenario. For the elements from Ba to Hf, we assume that the *s*- and *r*-process contributions are scaled versions of the solar *s*- and *r*-process abundances. We quantify the relative fractions of *s*- and *r*-process material for each cluster and show that they provide an excellent fit to the observed abundances.

Subject headings: Galaxy: Abundances, Galaxy: Globular Clusters: Individual: Messier Number: M4, Galaxy: Globular Clusters: Individual: Messier Number: M5, Stars: Abundances

1. Introduction

Globular clusters continue to play a vital role in testing many aspects of stellar evolution and stellar nucleosynthesis. Observational and theoretical studies of globular clusters have focused heavily upon (1) the star-to-star light element abundance variations (Cottrell & Da Costa 1981; Langer & Hoffman 1995; Gratton et al. 2004), (2) the cluster-to-cluster variation in the color distribution of horizontal branch stars, the so-called "2nd parameter effect" (Sandage & Wildey 1967; Lee et al. 1994; Carretta et al. 2006), and (3) the multiple populations as inferred from large spreads in metallicity and/or detailed structure in color-magnitude diagrams (Butler et al. 1978; Norris & Da Costa 1995; Bekki & Norris 2006).

Abundance measurements of the *s*-process and *r*-process elements offer great insight into stellar nucleosynthesis and globular cluster chemical evolution. Aside from M15, a metal-poor cluster that displays a scaled-solar *r*-process abundance distribution (Sneden et al.

1997, 2000; Otsuki et al. 2006), in general only a handful of s-process elements (e.g., Y, Zr, Ba, La) and the r-process element Eu have been measured in globular clusters.

The globular clusters M4 and M5 are particularly well suited for refining our understanding of stellar evolution and stellar nucleosynthesis, especially for the neutron-capture elements. Ivans et al. (1999, 2001) showed that these clusters have essentially identical metallicities, [Fe/H] = −1.2, based on high resolution spectra of large samples, 36 stars in each cluster. They also showed that the abundance similarities for these clusters extend to numerous α- and Fe-peak elements as well as the r-process element Eu. However, the s-process elements revealed striking abundance differences between these two clusters. Specifically, the heavy s-process elements Ba and La are overabundant in M4 relative to M5 (Ivans et al. 1999, 2001). With the notable exception of ω Cen, M4 may be uniquely enriched in s-process elements among the Galactic globular clusters (Pritzl et al. 2005).

Yong et al. (2008) recently extended the analysis of neutron-capture elements in these two clusters to Rb and Pb, s-process elements which may be overproduced in metal-poor asymptotic giant branch (AGB) stars (Busso et al. 1999; Travaglio et al. 2001). Whereas Pb production is dominated by 2 to $4M_{\odot}$ low-metallicity AGB stars (Travaglio et al. 2001), the intermediate-mass 4 to $8M_{\odot}$ AGB stars are predicted to dominate Rb production (van Raai et al. 2008). Not surprisingly, M4 again had higher abundance ratios [Rb/Fe] and [Pb/Fe] than M5. However, the abundance ratios [Rb/X] for X = Y, Zr, and La were very similar in the two clusters indicating that the nature of the s-process products is very similar for both clusters but that M4 formed from gas with a higher concentration of these products. A comprehensive study of s-process elements in these two clusters promises to provide a novel observational study of the s-process at low metallicities as well as valuable clues to the chemical evolution diversity of globular clusters. In this paper we present such an analysis, focusing upon a suite of α-, Fe-peak, s-process, and r-process elements.

2. Observations and analysis

The sample consists of 12 bright giants in M4 and 2 bright giants in M5 observed with the high resolution spectrograph MIKE (Bernstein et al. 2003) on the Magellan Clay Telescope. These are the same high quality spectra analyzed by Yong et al. (2008) (R = 55,000, wavelength coverage from 3800Å to 8500Å, and S/N = 140 per resolution element at 4000Å and S/N = 800 per resolution element at 7800Å).

The stellar parameters are presented in Table 1 and were determined using a traditional spectroscopic approach. Equivalent widths (EWs) for a set of Fe lines were measured using

routines in IRAF[1]. We used the local thermodynamic equilibrium (LTE) stellar line analysis program MOOG (Sneden 1973) and LTE model atmospheres from the Kurucz (1993) grid to derive an abundance for a given line. The effective temperature, $T_{\rm eff}$, was adjusted until the abundances from Fe I lines displayed no trend with the lower excitation potential. The surface gravity, $\log g$, was adjusted until the abundances from Fe I and Fe II lines were in agreement. The microturbulent velocity, ξ_t, was adjusted until there was no trend between the abundances from Fe I lines and EW. This process was iterated until self consistent stellar parameters were obtained. Ideally, the trends between abundance and EW and between abundance and lower excitation potential should be exactly zero. Further, the abundances $\log \epsilon$(Fe I) and $\log \epsilon$(Fe II) should be exactly the same. In our analysis, we explored stellar parameters at discrete values. For $T_{\rm eff}$, we considered values at every 25 K (e.g., 4000 K, 4025 K, etc), for $\log g$, we considered values at every 0.05 dex (e.g., 1.00 dex, 1.05 dex, etc), and for ξ_t, we considered values at every 0.05 km s^{-1} (e.g., 1.70 km s^{-1}, 1.75 km s^{-1} etc). We assumed that excitation equilibrium was satisfied when the slope between $\log \epsilon$(Fe I) and lower excitation potential was ≤ 0.004. We assumed that ionization equilibrium was achieved when $|\log \epsilon$(Fe I) $- \log \epsilon$(Fe II) $| \leq 0.02$ dex. The microturbulent velocity was set when the slope between $\log \epsilon$(Fe I) and reduced equivalent width ($\log W/\lambda$) was ≤ 0.004. Our stellar parameters are in good agreement with Ivans et al. (1999, 2001). We estimate that the internal errors are $T_{\rm eff}$ $\pm$ 50 K, $\log g$ $\pm$ 0.2 dex, and ξ_t $\pm$ 0.2 km s^{-1}. For further details regarding the observations, data reduction, and derivation of stellar parameters, see Yong et al. (2008).

Whenever possible, the abundances for additional elements were determined via equivalent width analysis. For particular lines, the abundances were determined by generating synthetic spectra using MOOG and adjusting the abundance to match the observed spectrum. In Figures 1 to 4, we show examples of the abundance determination via synthetic spectra. When required, isotopic and/or hyperfine splitting was taken into account. For Pr, we were unable to obtain sufficient information to appropriately treat the hyperfine splitting. The EWs for the 5322.76Å Pr II line range from 24.6 to 65.4 mÅ and we caution that the abundances may be slightly overestimated. The line list, source of gf values, and EWs are given in Table 2. The adopted solar abundances are given in Table 3. The final abundances are presented in Tables 4 and 5. The abundances for Rb, Y, Zr, La, Eu, and Pb were taken from Yong et al. (2008). The abundance dependences upon the model parameters are given in Table 6.

[1]IRAF (Image Reduction and Analysis Facility) is distributed by the National Optical Astronomy Observatory, which is operated by the Association of Universities for Research in Astronomy, Inc., under contract with the National Science Foundation.

For the elements Si, Ca, Sc, Ti, V, Fe, Ni, La, and Eu, our mean abundances [X/Fe] and [Fe/H] for M4 and for M5 are in good agreement with the mean cluster values measured by Ivans et al. (1999, 2001) (see Figure 5). For Mn and Cu, our mean abundances [X/Fe] for M4 and M5 are also in good agreement with the mean cluster values measured by Sobeck et al. (2006) and Simmerer et al. (2003) respectively, who used the same spectra and stellar parameters as Ivans et al. (1999, 2001). For all elements previously measured in these clusters, the mean abundance differences are $\Delta[\mathrm{A/B}]_{\mathrm{(This\ study\ -\ Literature)}} = 0.08$ dex ($\sigma = 0.08$ dex) and 0.09 dex ($\sigma = 0.10$ dex) for M4 and M5 respectively. However, when we consider the mean cluster abundance differences, $([\mathrm{A/B}]^{\mathrm{M4}}_{\mathrm{This\ study}} - [\mathrm{A/B}]^{\mathrm{M5}}_{\mathrm{This\ study}})$ $-$ $([\mathrm{A/B}]^{\mathrm{M4}}_{\mathrm{Literature}} - [\mathrm{A/B}]^{\mathrm{M5}}_{\mathrm{Literature}})$, our results are in excellent agreement, -0.01 dex ($\sigma =$ 0.06 dex), with Ivans et al. (1999, 2001), Sobeck et al. (2006), and Simmerer et al. (2003). The similarity in the abundance differences, M4 $-$ M5, between the various studies highlights the differential nature of the analyses. That is, the various studies have derived abundances for stars in M4 and M5, that cover a small range of stellar parameters, using homogeneous spectra and analysis techniques. While the similarity in abundance differences is very pleasing, it is not unexpected. We will take advantage of the very precise abundance differences to explore the chemical similarities and differences between these two clusters.

3. Results

In Figures 6 to 8, the upper panels show the mean abundances [X/Fe] and [Fe/H] for M4 and M5 and the lower panels show the abundance differences, $\Delta[\mathrm{A/B}] = [\mathrm{A/B}]_{\mathrm{M4}} - [\mathrm{A/B}]_{\mathrm{M5}}$. The error bars in these figures represent the observed spread (σ) in the measured abundances. We note that the observed spread in the measured abundances is in excellent agreement with the predicted spread, $\sigma_{\mathrm{predicted}} - \sigma_{\mathrm{observed\ (M4)}} = 0.00$ ($\sigma = 0.05$) and $\sigma_{\mathrm{predicted}} - \sigma_{\mathrm{observed\ (M5)}} =$ 0.03 ($\sigma = 0.05$). For all elements in this study, we therefore regard the abundances as being constant within each cluster. (Note that the $\sigma_{\mathrm{predicted}}$, taken directly from Table 6, neglect errors due to EW measurements and continuum placement which may be small in our high quality spectra of moderately metal-poor stars. Further, these uncertainties only account for the relative internal uncertainties.) For M4, the light element Na was found to vary by $\Delta[\mathrm{Na/Fe}] = 0.62$ dex within our sample (Yong et al. 2008). In this study, we find that none of the abundance ratios [X/Fe] for X = Si to Th are correlated with [Na/Fe].

3.1. The α- and Fe-peak elements, Si to Zn

In Figure 6, we plot the abundance ratios [X/Fe] and [Fe/H] for various α- and Fe-peak elements from Si to Zn. We confirm the findings by Ivans et al. (1999, 2001) that M4 and M5 have very similar abundances of Ca, Sc, Ti, V, Fe, and Ni. Our results extend the abundance similarities to the elements Cr and Co. For every element between Ca and Ni inclusive, M4 and M5 have essentially identical compositions, $<\Delta[\mathrm{A/B}]_{(\mathrm{M4-M5})}> = 0.04$ ($\sigma = 0.06$). The remarkable abundance similarity between M4 and M5 for the elements from Ca to Ni is most readily seen in the lower panel of Figure 6. In Figures 9 to 11, we plot the spectra for M4 L1411 and M5 IV-81, two stars for which we derived very similar values of T_{eff}. Therefore, any difference between the spectra is most likely due to abundance differences between the two stars. In these figures, the similarities in the line strengths of Ca, Sc, Ti, V, Fe, and Co reinforce our findings that these abundances (and the stellar parameters) are very similar in the two stars.

The abundance similarities for M4 and M5 do not extend to the elements Si, Cu, and Zn. For these elements, M4 has [X/Fe] ratios roughly 0.3 dex higher than those in M5.

The case of Si was already documented by Ivans et al. (2001). In Figure 9, lines of Si show considerably different strengths in two stars with very similar values of T_{eff}, which supports the claim that the Si abundances differ between M4 L1411 and M5 IV-81. Curiously, the behavior of Si is very different from the other α-elements Ca and Ti.

The differences in Zn abundances between M4 L3209 and M5 IV-81 can be seen in Figure 2. Although the abundance differences are not immediately obvious when visually comparing line strengths in these two stars, synthetic spectra reveal that M4 L3209 is overabundant in Zn relative to M5 IV-81.

For the abundances of Cu, differences between M4 and M5 were reported by Simmerer et al. (2003). In Figure 1, the abundance differences between M4 L1411 and M5 IV-81 can be seen from the synthetic spectra. Simmerer et al. (2003) suggested that the [Cu/Fe] abundances in both clusters were in agreement with field stars at the same metallicity. (They found a 0.17 dex difference in [Fe/H] between these clusters with M4 being the more metal-rich cluster). Inspection of their Figure 6 shows that while [Cu/Fe] in halo field stars (drawn exclusively from Mishenina et al. 2002) appears to be falling rapidly with decreasing metallicity, there are no field stars in the metallicity regime between M4 and M5. The sparse data set reveal that for the five field halo stars closest in metallicity to M4 and M5, the [Cu/Fe] values cover roughly 0.6 dex. However, some of the Mishenina et al. (2002) comparison field halo stars may be regarded as being (slightly) chemically peculiar. HD 6833 has a higher than usual ratio [Zr/Fe] = +0.48 (Fulbright 2000) and HD 166161 has a higher than usual ratio

$\log \epsilon$(La/Eu) = 0.71 (Simmerer et al. 2004). For these two stars, the [Cu/Fe] ratios may not be representative of the general halo trend and therefore, the claim that M4 and M5 have Cu abundances in agreement with field halo stars needs to be re-examined. Recent Cu measurements by Primas & Sobeck (2008) more clearly define the [Cu/Fe] versus [Fe/H] trend in field halo stars. Their results suggest that the 0.25 dex difference in [Cu/Fe] between M4 and M5 may exceed the intrinsic spread for the small range in [Fe/H] spanned by the two clusters. However, we note that such abundance comparisons between different studies can be problematic due to (unknown) systematic differences.

3.2. The *s*-process and *r*-process elements, Rb to Th

In Figure 7, we plot the abundance ratios [X/Fe] for various *s*-process and *r*-process elements from Rb to Gd and in Figure 8, we plot the abundance ratios for all elements including Hf, Pb, and Th. Ivans et al. (1999, 2001) showed that the *s*-process elements Ba and La are overabundant in M4 relative to M5 and Yong et al. (2008) extended the abundance differences to the *s*-process elements Rb and Pb. We find that every *s*-process element shows overabundances in M4 relative to M5. In Figures 9 (Zr), 10 (Y and Mo), and 11 (Y, Zr, and Nd), various *s*-process elements have considerably different line strengths reinforcing the claim that the abundances differ between M4 L1411 and M5 IV-81. The nine *s*-process elements measured in M4 and M5, Rb, Sr, Y, Zr, Mo, Ba, La, Ce, and Pb, have $<\Delta[\mathrm{X/Fe}]_{(\mathrm{M4-M5})}> = 0.38$ ($\sigma = 0.14$). Although the abundances are derived from a single line in a crowded region, the behavior of Pb, $\Delta[\mathrm{Pb/Fe}]_{(\mathrm{M4-M5})} = 0.65$, may differ from that of the other *s*-elements in these clusters. Recent observations of Pb by Aoki & Honda (2008) in a sample of field halo stars without large carbon enhancements show that M5 has a [Pb/Fe] ratio comparable to field stars at the same metallicity. The Aoki & Honda (2008) results also show that the globular clusters NGC 6752 and M13 have [Pb/Fe] ratios typical of field halo stars at the same metallicity (Yong et al. 2006b).

The sole *r*-process element measured by Ivans et al. (1999, 2001) is Eu and was found to have a slightly higher abundance in M5 relative to M4, in contrast to the behavior of the *s*-elements. In this study, we have measured the abundances for three additional *r*-process elements, Sm, Gd, and Th. In Figure 4, we show synthetic spectra fits to the 5989Å Th II line in which M5 IV-81 has a slightly higher abundance than M4 L1411. The 5989Å Th II line was also used by Aoki et al. (2007) and Figure 4 shows that in the absence of large Th enhancements, abundance estimates are only possible from extremely high S/N spectra. Ivans et al. (2006) measured Th abundances in the *r*-process-rich star HD 221170 and found that the abundances from 5989Å Th II line agreed with measurements from other Th lines.

In Figure 11, the 4642Å Sm II line has similar strengths in M4 L1411 and M5 IV-81.

In Figure 7 there is a trend in which Δ[X/Fe]$_{(M4-M5)}$ decreases as the atomic number increases for the r-process elements Sm, Eu, and Gd. However, this trend does not extend to the Th abundances (see Figure 8). Overall, all four r-process elements, Sm, Eu, Gd, and Th, are slightly underabundant in M4 relative to M5, $<\Delta$[X/Fe]$_{(M4-M5)}> = -0.13$ ($\sigma = 0.09$).

For the neutron-capture elements Pr, Nd, and Hf, the solar abundances may be equally attributed to the s-process and r-process. Given the behavior of the s- and r-elemental abundances in these clusters, we would therefore expect Pr, Nd, and Hf to be overabundant in M4 relative to M5, but that the magnitude of the enhancement would lie midway between the bulk of the s- and r- elements. Indeed, the abundance differences Δ[Pr/Fe]$_{(M4-M5)}$ = +0.09, Δ[Nd/Fe]$_{(M4-M5)}$ = +0.12, and Δ[Hf/Fe]$_{(M4-M5)}$ = +0.11, all lie midway between the heavy s-elements, $\Delta<$[Ba,La,Ce/Fe]$>_{(M4-M5)} = +0.36$, and the r-process elements $\Delta<$[Sm,Eu,Gd/Fe]$>_{(M4-M5)} = -0.12$. For Pr, these results indicate that either hyperfine structure does not significantly affect the abundances within our sample or that fortuitously, hyperfine structure equally affects the abundances in our sample.

4. Discussion

4.1. Background

In terms of chemical composition, globular clusters continue to present a series of intriguing questions concerning stellar nucleosynthesis and chemical evolution. This paper examines the pair of clusters - M4 and M5 - and has confirmed and extended the observations of differences in composition for these clusters of very similar iron abundances. Of the elements examined by us up through the Fe-peak, three are more abundant in M4 than in M5: Si, Cu, and Zn. Differences in [X/Fe] are 0.2 to 0.3 dex and might be the same for all three elements. There are abundance differences for the heavy elements Rb to Th that range from +0.6 (Pb) to −0.2 (Gd). It is from these abundance differences that we develop our speculations about stellar nucleosynthesis and chemical evolution.

Determinations of the compositions of globular cluster stars suggest the following chemical history for a cluster. The present population of stars formed from a gas cloud of homogeneous composition; this postulate is necessary to account for the fact that within a given cluster all stars have the same iron abundance (and many other elemental abundances). Within a cluster, there are star-to-star differences in the abundances of light elements from C to Al. Discovery of O, Na, and Al abundance differences among turn-off and subgiant stars (e.g., Gratton et al. 2001) proves that a cause is to be found in the cluster's local envi-

ronment. A possibility, often cited and explored, involves the selective accretion or pollution of material from the winds of AGB stars, particularly highly luminous intermediate-mass AGB stars with hot-bottom convective envelopes capable of nucleosynthesis of C to Al (e.g., Cottrell & Da Costa 1981; Denissenkov et al. 1998; Ventura et al. 2001), although there are quantitative problems with this scenario (Denissenkov & Herwig 2003; Fenner et al. 2004; Karakas et al. 2006a). Undoubtedly, an additional contribution to the abundance variations involving C, N, Li, and possibly O in red giants is the presence of mixing into the atmosphere of nuclear-processed material from the interior. If the convective mixing, expected to a certain degree of every red giant, is additionally dependent on a stellar property such as rotation, star-to-star differences in composition will result for the red giants.

Given this background, we offer the following idea for the primary origin of the composition differences between M4 and M5. Since the abundances of Si, Cu, Zn, and the heavier elements do not show a star-to-star spread across the M4 sample, we suppose that there is no detectable (positive or negative) contribution to their abundances from the polluting stars responsible for the star-to-star abundance variations, and, therefore, the abundance differences were present between the clouds forming these two clusters.

In the case of M5 and many other globular clusters, the relative abundances (i.e., the [X/Fe] ratios) of the elements unaffected by either mixing in red giants or accretion of pollutants from winds of AGB stars (or other sources) fall within the range exhibited by field stars of the same iron abundance (e.g., Gratton et al. 2004 and Pritzl et al. 2005). This congruence suggests that most globular clusters form from a cloud that underwent the same pattern of chemical evolution that led to the majority of the field halo stars.

The implications of this suggestion will not be thoroughly explored here but two points will be mentioned. One possibility is that field halo stars were constituents of globular clusters but some stars, now field stars, may have been ejected from the present population of clusters. Indeed, the globular clusters Pal 5, NGC 5466, and NGC 6712 exhibit large tidal tails and/or other evidence of severe tidal disruption (de Marchi et al. 1999; Odenkirchen et al. 2001; Belokurov et al. 2006). However, while Pal 5 shows the globular cluster signature of light element abundance variations (Smith et al. 2002), such abundance patterns have yet to be found in field halo stars (Gratton et al. 2000). Alternatively, the process of cluster formation may have resulted in the dispersal of stars rather than a stable cluster. Additionally, the suggestion places constraints on the chemical evolution histories of gas clouds from which clusters and field stars formed. In the case of metal-poor clusters including M4 and M5 and field stars of comparable metallicity, chemical evolution was dominated by ejecta from Type II supernovae; Type Ia supernovae have almost certainly not made their distinctive contributions to the composition of the gas cloud. Similarity in

[X/Fe] ratios implies similarities in the mixing of ejecta with ambient gas over the history of the clouds from which field and cluster stars formed. For elements where [X/Fe] ratios in the ejecta are not very sensitive to the initial mass function or the initial composition (i.e., the α-elements), different levels of mixing with pristine gas uncontaminated by X and Fe, or mixing with gas previously polluted by ejecta from Type II supernovae (same [X/Fe] but different [Fe/H]), will give essentially a single value of [X/Fe] at all [Fe/H]. On the other hand, for elements like Cu where the yield is dependent on the initial composition of the massive stars, variations in the mixing processes will lead to a broadening of the [Cu/Fe] versus [Fe/H] relation.

With this introduction we turn to discussion of the abundance differences between M4 and M5.

4.2. The *s*- and *r*-process mix: Ba to Th

With the usual attribution of Ba to the *s*-process and Eu to the *r*-process, the higher [Ba/Fe] and the lower [Eu/Fe] for M4 relative to M5 indicates that the M4 stars formed from gas that was enriched in *s*-process products but deficient in *r*-process products relative to the mixtures in the gas that formed the M5 stars. This attribution may be subject to quantitative analysis with two assumptions. It has been shown that relative abundances of *r*-process products in the interval Ba to Ir in *r*-process enriched stars (e.g., Sneden et al. 1996; Westin et al. 2000; Christlieb et al. 2004) and in the globular cluster M15 (Sneden et al. 1997, 2000; Otsuki et al. 2006) closely follows the distribution of *r*-process products derived from solar system abundances. This observation that the *r*-process from Ba to Ir is 'universal' remains without convincing theoretical explanation. Observations show that universality does not extend to the lighter elements - Rb to Mo are the observable elements. Our first assumption is that the *r*-process contributions to M4 and M5 are scaled versions of the solar *r*-process abundances. The second assumption is that the *s*-process contributions are scaled versions of the solar *s*-process abundances. Resolution of the solar abundances into *r*- and *s*-process contributions is taken from Simmerer et al. (2004). These assumptions are not validated by observations unlike the assumption about the *r*-process.

For M4 and M5, we adopted their mean abundance ratios [X/Fe]. We then took linear combinations of the solar *s*- and *r*-process abundances (adopting [Fe/H] = -1.25) exploring the full range of parameter space (i.e., considering values from 0.01 to 1.00 times the solar *s*- and *r*-process abundances). For each combination of *s*- and *r*-process abundances, we compared the predicted abundance ratios with the observed abundance ratios. For each cluster, we located the optimal scaling factors for the *s*- and *r*-process. When considering

the elements from Ba to Hf, we find s = 0.188 and r = 0.135 for M4 and s = 0.060 and r = 0.205 for M5 where 's' and 'r' are the scaling factors of the solar *s*- and *r*-process abundances respectively. For both clusters, the predicted and measured abundances are in very good agreement (see Figure 12). For M4 we find $\Delta[\mathrm{X/Fe}]_{\mathrm{predicted-observed}} = 0.04$ ($\sigma = 0.05$) and for M5 we find $\Delta[\mathrm{X/Fe}] = 0.02$ ($\sigma = 0.04$).

For both clusters, the abundances of Th lie above the predictions, albeit by similar amounts. The ratio of Th to Eu is identical in both clusters, [Th/Eu] = 0.11. Since Th and Eu are produced exclusively by the *r*-process, the identical [Th/Eu] ratios in M4 and M5 indicate that the *r*-process universality extends to Th in both clusters. Furthermore, the identical [Th/Eu] ratios suggests that no differential decay of Th has occurred and that these two clusters have essentially identical ages. (An uncertainty of 0.1 dex in the [Th/Eu] ratio would result in an age uncertainty of roughly 3 billion years.)

For both clusters, the observations of Pb fall below the predictions with M4 lying closer to the prediction than M5 owing to the different abundances, [Pb/Fe] = 0.30 in M4 and [Pb/Fe] = −0.35 in M5. As mentioned, the Pb abundance in M5 is typical of field halo stars at the clusters' metallicities. The cluster-to-cluster differences between the observed and predicted Pb abundances indicate that the *s*-process similarities break down for Pb. In the Sun, more than 50% of ^{208}Pb, the most abundant isotope, is due to the so-called "strong component" (e.g., Clayton & Rassbach 1967, Käppeler et al. 1989), where low mass metal-poor AGB stars are the likely site of this component. Therefore, the differences between the observed and predicted Pb abundances in M4 and M5 provide a hint that the sources of the *s*-process, in particular the strong component, differ between these clusters.

Had we included all elements from Ba to Th in determining the scaling factors for the solar *s*- and *r*-process abundances, we would have obtained very similar values (M4: s = 0.175, r = 0.138, and M5: s = 0.053, r = 0.210) as obtained when fitting the Ba to Hf abundances. These new predictions again provide a poor fit to Pb and Th.

The mix of *r*- and *s*-process contributions for M5 is typical of the mix found in halo field stars but the mix for M4 is quite atypical. This is well shown when considering the ratio of the La to Eu abundances. Inspection of Figure 7 in Simmerer et al. (2004) shows that M5, $\log \epsilon(\mathrm{La/Eu}) = 0.28$, is representative of field stars at the cluster's metallicity. However, M4, $\log \epsilon(\mathrm{La/Eu}) = 0.70$, is in the far tail of the distribution of La/Eu ratios for field stars and close to the stars labelled as *s*-process enriched. Yet, as our fits to the abundance patterns show, the *s*-process in M4 has the same pattern of abundances as in M5 and the Sun. Thus, no new site for *s*-process operation is needed to account for the M4-M5 differences, at least for the elements Ba to Hf. We presume that AGB stars are the active site. Yet, the difference in *s*-process pollution between M4 and M5 might suggest that M4 originated in a different

part of the Galaxy to M5 and local halo stars.

4.3. Cu to Zr

The successful dissection of the Ba-Ir abundances into different mixing fractions of solar-like r- and s-process abundance patterns cannot be easily extended to lighter elements in the Cu-Zr interval. This is likely attributable to the appearance of an additional one or more processes of stellar nucleosynthesis.

One expects the weak s-process to contribute to the elements Cu to Zr as revealed from the fit to the solar abundances (e.g., Käppeler et al. 1989). This neutron capture process occurs in massive stars in the He-burning and the C-burning shells with products ejected without substantial modification in the supernova explosion. At initial metallicities [Fe/H] ~ -1, the contributions from the He-burning shell appear to be more important than from the C-burning shell. This s-process does not provide significant yields beyond the cross-section bottleneck at the neutron magic number $N = 50$ and, thus, the Ba-Ir interval is unaffected by this contribution from massive stars. Predicted yields for this weak s-process are sketched by Pignatari & Gallino (2007). It is also below [Fe/H] ~ -1 that the weak s-process may become so ineffective that explosive Si-burning may replace it as the source of Cu, Zn, and other weak s-process products.

The r-process, whose site is probably the deep interior of Type II supernovae from massive stars, is likely to contribute also to the Cu-Zr interval, in part or in whole. Unfortunately, there are not even qualitative predictions about these r-process yields. Abundance analyses of very r-process enriched stars by Sneden and colleagues have shown a star-to-star variation in these lighter elements – Ga to Ag – in their abundance ratios with respect to the abundances of the heavier elements from Ba and up. These variations have been ascribed to 'a second r-process' but may at least in part reflect a weak s-process contribution from massive stars, also the likely site of the r-process(es). (Recall that we have discounted the possibility that Type Ia supernovae are contributing to the chemical evolution of M4 and M5 and field stars of comparable or lower metallicity.)

As expected, Figure 12 shows that predictions based on the scaling factors for the solar s- and r-process abundances that match the elements from Ba to Hf provide a poor fit to the elements from Rb to Mo. Had we included all elements from Rb to Th in the fit, the scaling factors would be essentially unchanged (M4: s = 0.060, r = 0.198, and M5: s = 0.188, r = 0.138), and the fit to the elements Rb to Mo would remain poor.

4.4. The case of Si

An overabundance of α-elements is commonly taken as the signature of gas contaminated to a major degree by ejecta of Type II supernovae. Here, the α-element directory includes O, Mg, Si, S, and Ca with Ti as an honorary member according to observers. Ca and Ti have very similar abundances in M4 and M5, but Si is definitely overabundant in M4 with respect to M5 (Figure 6 and Table 4). In M4, the overabundance of Mg, [Mg/Fe] = 0.56 (σ = 0.05) from 12 stars (Yong et al. 2008), is similar to that of Si, [Si/Fe] = 0.58 (σ = 0.08). This contradicts findings by Ivans et al. (2001) who found that stars in M4 have Si abundances about 0.2 dex higher than Mg. A more careful investigation of the difference in [Mg/Si] ratios in M4 by different authors would need to account for systematic differences.

Both clusters exhibit the classic signature of α-elements in metal-poor stars – [α/Fe] $\simeq$ 0.3 dex – but this signature is different in its details, as just noted. There is no obvious explanation for the enhanced Si abundances in M4. Si and Ca (as well as S and Ar) are all produced by incomplete explosive Si burning and explosive O burning in massive stars. Therefore, any Si excess in M4 relative to M5 should be accompanied by a similar Ca excess.

4.5. Comments on Cu and Zn nucleosynthesis

Pioneering measurements of Cu and Zn in field stars showed that between $-2.5 \leq$ [Fe/H] ≤ 0.0, [Cu/Fe] declined with decreasing metallicity whereas [Zn/Fe] was constant and solar (Peterson 1981; Gratton & Ortolani 1988; Sneden & Crocker 1988; Sneden et al. 1991). Although a large amount of data are now available for these elements, the nucleosynthetic origins of Cu and Zn remain unclear with both elements likely requiring multiple production sites and metallicity dependent yields. For Cu, Type Ia supernovae (Matteucci et al. 1993; Mishenina et al. 2002) and massive stars (Timmes et al. 1995; Romano & Matteucci 2007) are proposed to be the dominant producers with low mass AGB stars believed to provide only a minor contribution (Matteucci et al. 1993). For Zn, massive stars (Timmes et al. 1995) and Type Ia supernovae (Matteucci et al. 1993) have been suggested as being the major producers. Other potential sources of Zn include the weak s-process in massive stars and the main s-process in low mass AGB stars (Matteucci et al. 1993), and at very low metallicity, the s-process or r-process in massive stars (Umeda & Nomoto 2002; Heger & Woosley 2002).

The abundances measured in M4 and M5 offer additional insight into the production sites of Cu and Zn. These metal-poor globular clusters were formed early in the history of our Galaxy, before Type Ia supernovae contributed to their chemical evolution. Therefore, our measurements confirm that stars other than Type Ia supernovae must produce significant

amounts of Cu and Zn at low metallicities. Abundance differences of roughly 0.3 dex are found for the α-element Si (produced primarily in massive stars) as well as the s-process elements (produced in AGB stars or massive stars). In light of the abundance differences for Cu and Zn in these two clusters, we now examine the synthesis of Cu and Zn in massive stars and AGB stars based on recent theoretical models.

4.5.1. Massive star production

Both the stable isotopic nuclei of Cu and the five of Zn are produced, at low metallicities ([Fe/H] < -1), only by the complete explosive Si burning, i.e., in the deepest regions of the exploding star where the peak temperature exceeds 5×10^9 K and therefore matter can reach the nuclear statistical equilibrium (Chieffi & Limongi 2004). The striking similarities of the relative abundances of the elements between Ca and Ni seem to clearly indicate that the core collapse supernovae responsible for the bulk production of the nuclei in this range are very similar in M4 and M5. In this respect Cu and Zn should also behave similarly (because of their production site) but there is a "caveat": they are less abundant (relative to hydrogen) than Co and Ni and hence they would be the first elements within the Fe peak nuclei to be modified by the passage of a neutron flux.

In massive stars, He- and C-burning can lead to activation of the ^{22}Ne(α,n)^{25}Mg neutron source whose high neutron densities are responsible for synthesizing s-process elements up to Sr (Busso et al. 1999). If the weak s-process is solely responsible for the enhanced Cu and Zn in M4, we would expect the abundances of Rb relative to nearby elements such as Sr, Y, and Zr to also differ between these clusters (Tomkin & Lambert 1983; Lambert et al. 1995; Abia et al. 2001). Observation support for this scenario comes from enhanced Rb abundances in luminous Galactic OH/IR stars of solar metallicity (García-Hernández et al. 2006) that are matched by theoretical models (van Raai et al. 2008). However, Yong et al. (2008) showed that in M4 and M5 the ratio [Rb/Zr] was identical within the measurement uncertainties and therefore, it may be difficult to ascribe any difference in Cu and Zn solely to the weak s-process, unless the production of [Rb/Zr] has a metallicity dependence and is not significant at low metallicity. As discussed above, no comprehensive predictions are presently available.

4.5.2. AGB production

Models presented in Karakas et al. (2008) indicate that Zn, in general, is not altered by AGB nucleosynthesis. Zn can be produced in the most massive, lowest metallicity AGB stars, with the largest abundance predicted to be [Zn/Fe] $\sim$ 0.4 dex in a $5M_{\odot}$, $Z = 0.004$ model. The total expelled mass of Zn in this case is small ($\sim 10^{-6}M_{\odot}$). Preliminary results for Cu suggest that neutron-capture nucleosynthesis in intermediate-mass low-metallicity AGB stars could be an extra production site for this element. Both stable isotopes of Cu are predicted to be enhanced in the He-shell of 4 to $8M_{\odot}$ AGB stars, with the final elemental Cu surface abundance estimated to be [Cu/Fe] $\sim$ 0.8 dex in a $5M_{\odot}$, $Z = 0.004$ model.

The results for Zn agree with the Travaglio et al. (2004) predictions that only 2.4% of elemental Zn comes from the *s* process, however the results for Cu are less clear, where Travaglio et al. (2004) estimate that 5.2% of Cu is produced in AGB stars. We would need to include updated AGB yields of Cu and Zn in a chemical evolution model to study the consistency with the Travaglio et al. (2004) results, as well as to determine just how efficient intermediate-mass AGB production really is, along with an exhaustive study of the many uncertainties affecting the AGB nucleosynthesis models. For example, one of the largest uncertainties is the mass-loss law used in the calculations, as this determines the number of third dredge-up mixing episodes. If the number of mixing episodes were to be halved, then about four times less Cu would be produced in the 5 $M_{\odot}$ example given above.

If $5M_{\odot}$ metal-poor AGB stars are solely responsible for the enhanced Cu and Zn in M4, we would expect differences in the abundances of the heavy Mg isotopes between M4 and M5 (Karakas & Lattanzio 2003; Karakas et al. 2006b). Observations of high ^{26}Mg/^{24}Mg ratios in field and cluster stars confirm the AGB yields (Gay & Lambert 2000; Yong et al. 2003a,b). Although the resolution is less than ideal (R = 55,000 in this study compared with R $\geq$ 90,000 in our previous studies of Mg isotope ratios in giant stars in globular clusters), we have measured the Mg isotope ratios using the same methods as Yong et al. (2003a, 2006a). The ratios are given in Table 7 and examples of synthetic spectra fits are shown in Figure 13. Given the resolution, we adopt ^{25}Mg = ^{26}Mg in the reported ratios, and therefore we regard these results as preliminary because our analyses of stars in other globular clusters have showed that ^{25}Mg and ^{26}Mg can behave independently. The uncertainties in the ratios are $b \pm 5$ and $c \pm 5$ when expressing the ratio as ^{24}Mg:^{25}Mg:^{26}Mg = $(100-b-c)$:b:c. Nevertheless, these preliminary results provide important additional information into the chemical evolution of these clusters. Within M4 and M5, the Mg isotope ratios are constant, in contrast to what is seen in the more metal-poor globular clusters NGC 6752 and M13 (Shetrone 1996; Yong et al. 2003a, 2006a). Given the small amplitude [Al/Fe] variation in our sample (Δ[Al/Fe]$_{\rm M4}$ = 0.23 compared with Δ[Al/Fe]$_{\rm NGC\ 6752}$ = 1.06), it is not surprising that the

Mg isotope ratios show a smaller variation in M4 than in NGC 6752 (and M13). In both M4 and M5, the ratios are very similar with a typical cluster ratio comparable to the solar value, ^{24}Mg:^{25}Mg:^{26}Mg = 80:10:10. Even at our resolution, the isotope ratios ^{25}Mg/^{24}Mg and ^{26}Mg/^{24}Mg in M4 and M5 exceed values measured in field halo stars at the clusters' metallicities (Gay & Lambert 2000; Yong et al. 2003b; Meléndez & Cohen 2007) and predictions from chemical evolution models (Alibés et al. 2001; Fenner et al. 2003). For example, the halo dwarf Gmb 1830 has [Fe/H] = −1.30 and ^{24}Mg:^{25}Mg:^{26}Mg = 94:3:3 (Tomkin & Lambert 1980). Therefore, the clouds from which M4 and M5 formed were not like the clouds from which halo stars like Gmb 1830 formed. In summary, the Mg isotope ratios in M4 and M5 do not support the scenario in which intermediate AGB stars are responsible for the Cu and Zn abundance differences between these clusters. For both clusters the isotope ratios exceed the values found in field stars at the same metallicity.

Further constraints on the AGB contribution to the Cu abundance differences in M4 and M5 come from the most massive globular cluster, ω Centauri. In ω Cen, Cunha et al. (2002) found a roughly constant ratio [Cu/Fe] $\simeq -0.5$ as [Fe/H] ranged from −2.0 to −0.8 in their sample of 40 stars. The same sample was previously analyzed by Norris & Da Costa (1995) who found that the abundance ratios [X/Fe] for *s*-process elements increased as [Fe/H] increases. Therefore, the low-mass AGB stars presumably responsible for the increasing [*s*-element/Fe] as [Fe/H] increases do not synthesize Cu. However, ω Cen exhibits a number of traits not found in other globular clusters. Detailed chemical evolution models such as those performed by Fenner et al. (2004) and Renda et al. (2004) will help unravel the origin of the Cu and Zn abundance differences in M4 and M5 as well as the synthesis of Cu and Zn in metal-poor stars.

4.6. Physical and kinematic differences between M4 and M5

Finally, we briefly consider the physical and kinematic parameters for M4 and M5. Within the Galactic globular clusters, M4 has a typical luminosity (i.e., mass), $M_V = -7.20$, while M5 is one of the more luminous (i.e., massive) clusters, $M_V = -8.81$ (Harris 1996, Feb. 2003 web version). The space velocities for these two clusters are considerably different. Dinescu et al. (1999) have shown that M5 has a very large apocentric radius ($R_a = 35.4$ kpc) while M4 has a very small apocentric radius ($R_a = 5.9$ kpc). Given that M4's orbit is confined to the inner disk and bulge, it would be of great interest to measure the abundances of Si, Cu, Zn, and *s*-process elements in a sample of inner disk and bulge stars at the metallicity of M4. Perhaps the elevated abundances of Si, Cu, Zn, and *s*-elements in M4 are representative of stars born at small Galactocentric radii. However, we note that Fulbright et al. (2007)

measured the abundances of Si, Ca, and Ti in bulge giants including four with $-1.5 \leq$ [Fe/H] ≤ -1.0. All have [Si/Fe] ratios comparable to [Ca/Fe] and [Ti/Fe]. Two stars below [Fe/H] $= -1$ in the Fulbright et al. (2007) sample have high [Al/Fe] and [Na/Fe] along with low [O/Fe], the abundance signature of hydrogen burning at high temperatures seen in globular clusters. Indeed, they speculate that these two stars may be members of the bulge globular cluster NGC 6522. Abundances of *s*-process elements were measured by McWilliam & Rich (1994) in three bulge giants with [Fe/H] ≤ -0.8, none of which showed *s*-process enrichments. Therefore, the enhanced abundances of Si and *s*-elements in M4 may not be representative of stars born at small Galactocentric radii.

5. Concluding remarks

In this paper we present abundance ratios [X/Fe] for a large number of α-, Fe-peak, *s*-process, and *r*-process elements for 12 bright giants in the globular cluster M4 and 2 bright giants of the globular cluster M5. This comprehensive abundance analysis is only possible due to the large wavelength coverage, high resolution, and very high S/N spectra. For all elements in this study, we find no evidence for star-to-star abundance variations in either cluster. We confirm and extend upon previous results for these clusters by showing that (1) for the elements from Ca to Ni, M4 and M5 have identical abundance ratios, (2) M4 shows overabundances by roughly 0.3 dex for Si, Cu, Zn, and all *s*-process elements relative to M5, and (3) for the *r*-process elements, M5 may have slightly higher abundances than M4 by 0.1 dex.

We also measure Mg isotope ratios and find that the ratios are solar in both clusters, with no sign of any star-to-star variation within each cluster. The ratios ^{25}Mg/^{24}Mg and ^{26}Mg/^{24}Mg exceed values found in field halo stars at the same metallicity, e.g., Gmb 1830, which implies differences in the clouds from which globular clusters and field halo stars formed. However, we regard these ratios as preliminary since the spectral resolution was insufficient to accurately distinguish ^{25}Mg from ^{26}Mg.

There is no clear explanation for the M4-M5 Si abundance differences since the abundances of Ca should, but do not, follow the behavior of Si. For the elements from Ba to Hf, we find that the mean abundances in M4 and M5 are well explained by scaled versions of the solar *s*- and *r*-process abundances, albeit with different mixes of *s*- and *r*-process material for each cluster. Therefore, no new *s*-process site is required to explain the M4-M5 abundance differences for the elements from Ba to Hf. However, although the Th abundances lie above these predictions, the ratio [Th/Eu] is identical in both clusters indicating that the universality of the *r*-process extends to Th in these clusters and that no differential decay of Th has

occurred, i.e., the clusters have identical ages. The Pb abundances lie below the predictions, by different amounts for each cluster. Therefore, the sources of the *s*-process may differ between M4 and M5, at least regarding the production of Pb via the strong component.

The abundance differences between M4 and M5 for Cu and Zn are particularly intriguing given that their nucleosynthetic origins continue to be debated. The *s*-process elements, produced in AGB stars (and massive stars), share a similar abundance behavior to Cu and Zn in M4 and M5. Updated, but preliminary, yields from AGB models indicate that small amounts of Zn may be produced only in the most massive AGB stars. These models also predict that the most massive AGB stars may produce Cu in contrast to our current understanding of Cu production. Massive AGB stars are expected to produce large amounts of the neutron-rich Mg isotopes, and observations of high ^{26}Mg/^{24}Mg ratios in field and cluster stars confirm the AGB yields. However, preliminary measurements show no difference in the Mg isotope ratios between these two clusters which constrains the contribution of intermediate-mass AGB stars to the Cu and Zn enhancements in M4. Si, which is produced in massive stars, shows a similar abundance behavior to Cu and Zn in M4 and M5. Cu and Zn may be produced in massive stars via the weak *s*-process. While the abundance ratios [Rb/Sr], [Rb/Y], and [Rb/Zr] are predicted to increase via the weak *s*-process, our measurements do not reveal any cluster-to-cluster variations in these abundance ratios which suggests that either massive stars are not responsible for the Cu and Zn differences or that metal-poor massive stars do not alter the [Rb/Zr] ratio. Of great interest would be detailed chemical evolution modeling of these two clusters to gain insight into the origin of the Cu and Zn abundance differences and therefore their nucleosynthesis production sites.

This research has made use of the SIMBAD database, operated at CDS, Strasbourg, France and NASA's Astrophysics Data System. DY thanks Inese Ivans and John Norris for valuable discussions and the referee for helpful comments. AIK acknowledges support from the Australian Research Council's Discovery Projects funding scheme (project number DP0664105), and thanks Maria Lugaro for help in developing the extended nucleosynthesis network. DLL thanks the Robert A. Welch Foundation of Houston for support. This research was supported in part by NASA through the American Astronomical Society's Small Research Grant Program.

REFERENCES

Abia, C., Busso, M., Gallino, R., Domínguez, I., Straniero, O., & Isern, J. 2001, ApJ, 559, 1117

Alibés, A., Labay, J., & Canal, R. 2001, A&A, 370, 1103

Aoki, W. & Honda, S. 2008, PASJ in press (arXiv:0804.0952)

Aoki, W., Honda, S., Sadakane, K., & Arimoto, N. 2007, PASJ, 59, L15

Asplund, M., Grevesse, N., & Sauval, A. J. 2005, in ASP Conf. Ser. 336: Cosmic Abundances as Records of Stellar Evolution and Nucleosynthesis, ed. T. G. Barnes, III & F. N. Bash, 25

Bekki, K. & Norris, J. E. 2006, ApJ, 637, L109

Belokurov, V., Evans, N. W., Irwin, M. J., Hewett, P. C., & Wilkinson, M. I. 2006, ApJ, 637, L29

Bernstein, R., Shectman, S. A., Gunnels, S. M., Mochnacki, S., & Athey, A. E. 2003, in Instrument Design and Performance for Optical/Infrared Ground-based Telescopes. Edited by Iye, Masanori; Moorwood, Alan F. M. Proceedings of the SPIE, Volume 4841, pp. 1694-1704 (2003)., 1694–1704

Busso, M., Gallino, R., & Wasserburg, G. J. 1999, ARA&A, 37, 239

Butler, D., Dickens, R. J., & Epps, E. 1978, ApJ, 225, 148

Carretta, E., Bragaglia, A., Gratton, R. G., Leone, F., Recio-Blanco, A., & Lucatello, S. 2006, A&A, 450, 523

Chieffi, A. & Limongi, M. 2004, ApJ, 608, 405

Christlieb, N., Beers, T. C., Barklem, P. S., Bessell, M., Hill, V., Holmberg, J., Korn, A. J., Marsteller, B., Mashonkina, L., Qian, Y.-Z., Rossi, S., Wasserburg, G. J., Zickgraf, F.-J., Kratz, K.-L., Nordström, B., Pfeiffer, B., Rhee, J., & Ryan, S. G. 2004, A&A, 428, 1027

Clayton, D. D. & Rassbach, M. E. 1967, ApJ, 148, 69

Cohen, J. G. & Meléndez, J. 2005, AJ, 129, 303

Cottrell, P. L. & Da Costa, G. S. 1981, ApJ, 245, L79

Cunha, K., Smith, V. V., Suntzeff, N. B., Norris, J. E., Da Costa, G. S., & Plez, B. 2002, AJ, 124, 379

de Marchi, G., Leibundgut, B., Paresce, F., & Pulone, L. 1999, A&A, 343, L9

Den Hartog, E. A., Lawler, J. E., Sneden, C., & Cowan, J. J. 2003, ApJS, 148, 543

—. 2006, ApJS, 167, 292

Denissenkov, P. A., Da Costa, G. S., Norris, J. E., & Weiss, A. 1998, A&A, 333, 926

Denissenkov, P. A. & Herwig, F. 2003, ApJ, 590, L99

Dinescu, D. I., Girard, T. M., & van Altena, W. F. 1999, AJ, 117, 1792

Fenner, Y., Campbell, S., Karakas, A. I., Lattanzio, J. C., & Gibson, B. K. 2004, MNRAS, 353, 789

Fenner, Y., Gibson, B. K., Lee, H.-c., Karakas, A. I., Lattanzio, J. C., Chieffi, A., Limongi, M., & Yong, D. 2003, PASA, 20, 340

Fulbright, J. P. 2000, AJ, 120, 1841

Fulbright, J. P., McWilliam, A., & Rich, R. M. 2007, ApJ, 661, 1152

García-Hernández, D. A., García-Lario, P., Plez, B., D'Antona, F., Manchado, A., & Trigo-Rodríguez, J. M. 2006, Science, 314, 1751

Gay, P. L. & Lambert, D. L. 2000, ApJ, 533, 260

Gratton, R., Sneden, C., & Carretta, E. 2004, ARA&A, 42, 385

Gratton, R. G., Bonifacio, P., Bragaglia, A., Carretta, E., Castellani, V., Centurion, M., Chieffi, A., Claudi, R., Clementini, G., D'Antona, F., Desidera, S., François, P., Grundahl, F., Lucatello, S., Molaro, P., Pasquini, L., Sneden, C., Spite, F., & Straniero, O. 2001, A&A, 369, 87

Gratton, R. G. & Ortolani, S. 1988, A&AS, 73, 137

Gratton, R. G., Sneden, C., Carretta, E., & Bragaglia, A. 2000, A&A, 354, 169

Grevesse, N., Asplund, M., & Sauval, A. J. 2007, Space Science Reviews, 130, 105

Grevesse, N. & Sauval, A. J. 1998, Space Science Reviews, 85, 161

Harris, W. E. 1996, AJ, 112, 1487

Heger, A. & Woosley, S. E. 2002, ApJ, 567, 532

Ivans, I. I., Kraft, R. P., Sneden, C., Smith, G. H., Rich, R. M., & Shetrone, M. 2001, AJ, 122, 1438

Ivans, I. I., Simmerer, J., Sneden, C., Lawler, J. E., Cowan, J. J., Gallino, R., & Bisterzo, S. 2006, ApJ, 645, 613

Ivans, I. I., Sneden, C., Kraft, R. P., Suntzeff, N. B., Smith, V. V., Langer, G. E., & Fulbright, J. P. 1999, AJ, 118, 1273

Käppeler, F., Beer, H., & Wisshak, K. 1989, Reports of Progress in Physics, 52, 945

Karakas, A. I., Fenner, Y., Sills, A., Campbell, S. W., & Lattanzio, J. C. 2006a, ApJ, 652, 1240

Karakas, A. I. & Lattanzio, J. C. 2003, PASA, 20, 279

Karakas, A. I., Lugaro, M., van Raai, M., Sterling, N. C., & Dinnerstein, H. L. 2008, ApJ submitted

Karakas, A. I., Lugaro, M. A., Wiescher, M., Görres, J., & Ugalde, C. 2006b, ApJ, 643, 471

Kurucz, R. 1993, ATLAS9 Stellar Atmosphere Programs and 2 km/s grid. Kurucz CD-ROM No. 13. Cambridge, Mass.: Smithsonian Astrophysical Observatory, 1993., 13

Kurucz, R. & Bell, B. 1995, Atomic Line Data (R.L. Kurucz and B. Bell) Kurucz CD-ROM No. 23. Cambridge, Mass.: Smithsonian Astrophysical Observatory, 1995., 23

Lambert, D. L., Smith, V. V., Busso, M., Gallino, R., & Straniero, O. 1995, ApJ, 450, 302

Langer, G. E. & Hoffman, R. D. 1995, PASP, 107, 1177

Lawler, J. E., Den Hartog, E. A., Sneden, C., & Cowan, J. J. 2006, ApJS, 162, 227

Lawler, J. E., Hartog, E. A. D., Labby, Z. E., Sneden, C., Cowan, J. J., & Ivans, I. I. 2007, ApJS, 169, 120

Lee, Y.-W., Demarque, P., & Zinn, R. 1994, ApJ, 423, 248

Matteucci, F., Raiteri, C. M., Busson, M., Gallino, R., & Gratton, R. 1993, A&A, 272, 421

McWilliam, A. & Rich, R. M. 1994, ApJS, 91, 749

Meléndez, J. & Cohen, J. G. 2007, ApJ, 659, L25

Mishenina, T. V., Kovtyukh, V. V., Soubiran, C., Travaglio, C., & Busso, M. 2002, A&A, 396, 189

Nilsson, H., Zhang, Z. G., Lundberg, H., Johansson, S., & Nordström, B. 2002, A&A, 382, 368

Norris, J. E. & Da Costa, G. S. 1995, ApJ, 447, 680

Norris, J. E., Da Costa, G. S., & Tingay, S. J. 1995, ApJS, 99, 637

Odenkirchen, M., Grebel, E. K., Rockosi, C. M., Dehnen, W., Ibata, R., Rix, H.-W., Stolte, A., Wolf, C., Anderson, Jr., J. E., Bahcall, N. A., Brinkmann, J., Csabai, I., Hennessy, G., Hindsley, R. B., Ivezić, Ž., Lupton, R. H., Munn, J. A., Pier, J. R., Stoughton, C., & York, D. G. 2001, ApJ, 548, L165

Otsuki, K., Honda, S., Aoki, W., Kajino, T., & Mathews, G. J. 2006, ApJ, 641, L117

Peterson, R. C. 1981, ApJ, 244, 989

Pignatari, M. & Gallino, R. 2007, Memorie della Societa Astronomica Italiana, 78, 543

Primas, F. & Sobeck, J. 2008, in American Institute of Physics Conference Series, Vol. 1001, Evolution and Nucleosynthesis in AGB Stars, 230–234

Pritzl, B. J., Venn, K. A., & Irwin, M. 2005, AJ, 130, 2140

Prochaska, J. X., Naumov, S. O., Carney, B. W., McWilliam, A., & Wolfe, A. M. 2000, AJ, 120, 2513

Ramírez, S. V. & Cohen, J. G. 2002, AJ, 123, 3277

Reddy, B. E., Tomkin, J., Lambert, D. L., & Allende Prieto, C. 2003, MNRAS, 340, 304

Renda, A., Fenner, Y., Gibson, B. K., Karakas, A. I., Lattanzio, J. C., Campbell, S., Chieffi, A., Cunha, K., & Smith, V. V. 2004, MNRAS, 354, 575

Romano, D. & Matteucci, F. 2007, MNRAS, 378, L59

Sandage, A. & Wildey, R. 1967, ApJ, 150, 469

Shetrone, M. D. 1996, AJ, 112, 2639

Simmerer, J., Sneden, C., Cowan, J. J., Collier, J., Woolf, V. M., & Lawler, J. E. 2004, ApJ, 617, 1091

Simmerer, J., Sneden, C., Ivans, I. I., Kraft, R. P., Shetrone, M. D., & Smith, V. V. 2003, AJ, 125, 2018

Smith, G. H., Sneden, C., & Kraft, R. P. 2002, AJ, 123, 1502

Smith, V. V., Suntzeff, N. B., Cunha, K., Gallino, R., Busso, M., Lambert, D. L., & Straniero, O. 2000, AJ, 119, 1239

Sneden, C. 1973, ApJ, 184, 839

Sneden, C. & Crocker, D. A. 1988, ApJ, 335, 406

Sneden, C., Gratton, R. G., & Crocker, D. A. 1991, A&A, 246, 354

Sneden, C., Johnson, J., Kraft, R. P., Smith, G. H., Cowan, J. J., & Bolte, M. S. 2000, ApJ, 536, L85

Sneden, C., Kraft, R. P., Shetrone, M. D., Smith, G. H., Langer, G. E., & Prosser, C. F. 1997, AJ, 114, 1964

Sneden, C., McWilliam, A., Preston, G. W., Cowan, J. J., Burris, D. L., & Armosky, B. J. 1996, ApJ, 467, 819

Sobeck, J. S., Ivans, I. I., Simmerer, J. A., Sneden, C., Hoeflich, P., Fulbright, J. P., & Kraft, R. P. 2006, AJ, 131, 2949

Timmes, F. X., Woosley, S. E., & Weaver, T. A. 1995, ApJS, 98, 617

Tomkin, J. & Lambert, D. L. 1980, ApJ, 235, 925

—. 1983, ApJ, 273, 722

Travaglio, C., Gallino, R., Arnone, E., Cowan, J., Jordan, F., & Sneden, C. 2004, ApJ, 601, 864

Travaglio, C., Gallino, R., Busso, M., & Gratton, R. 2001, ApJ, 549, 346

Umeda, H. & Nomoto, K. 2002, ApJ, 565, 385

van Raai, M. A., Lugaro, M., Karakas, A. I., & García-Hernández, D. A. 2008, in American Institute of Physics Conference Series, Vol. 1001, Evolution and Nucleosynthesis in AGB Stars, 146–153

Ventura, P., D'Antona, F., Mazzitelli, I., & Gratton, R. 2001, ApJ, 550, L65

Westin, J., Sneden, C., Gustafsson, B., & Cowan, J. J. 2000, ApJ, 530, 783

Yong, D., Aoki, W., & Lambert, D. L. 2006a, ApJ, 638, 1018

Yong, D., Aoki, W., Lambert, D. L., & Paulson, D. B. 2006b, ApJ, 639, 918

Yong, D., Grundahl, F., Lambert, D. L., Nissen, P. E., & Shetrone, M. D. 2003a, A&A, 402, 985

Yong, D., Lambert, D. L., & Ivans, I. I. 2003b, ApJ, 599, 1357

Yong, D., Lambert, D. L., Paulson, D. B., & Carney, B. W. 2008, ApJ, 673, 854

Table 1. Stellar parameters.

Star	$T_{\rm eff}$	$\log g$	ξ_t	[Fe/H]
M4 L1411	4025	0.80	1.75	−1.23
M4 L1501	4175	1.00	1.55	−1.29
M4 L1514	3950	0.30	1.85	−1.22
M4 L2307	4125	0.95	1.65	−1.19
M4 L2406	4150	0.15	2.20	−1.30
M4 L2617	4275	1.25	1.65	−1.20
M4 L3209	4075	0.75	1.95	−1.25
M4 L3413	4225	1.10	1.75	−1.23
M4 L3624	4225	1.05	1.60	−1.29
M4 L4511	4150	1.05	1.70	−1.22
M4 L4611	3925	0.15	1.45	−1.09
M4 L4613	3900	0.20	1.70	−1.25
M5 IV-81	4050	0.30	1.90	−1.28
M5 IV-82	4400	1.20	1.75	−1.33

Table 2. Equivalent widths [ONLINE ONLY].

Wavelength (Å)	Species	χ (eV)	$\log gf$	Source gf	M4 L1411	M4 L1501	M4 L1514	M4 L2307	M4 L2406	M4 L2617	M4 L3209	M4 L3413	M4 L3624	M4 L4511	M4 L4611	M4 L4613	M5 IV-81	N
5665.554	14.0	4.92	−2.04	RC02	49.2	46.6	44.3	50.1	55.7	40.6	48.8	43.1	46.5	50.4	51.3	45.2	35.1	
5690.430	14.0	4.93	−1.83	RC02	48.4	49.1	48.8	49.4	58.4	51.1	47.5	47.3	49.0	50.3	47.1	46.0	36.4	
5948.550	14.0	5.08	−1.23	RC02	76.3	80.3	77.0	82.1	100.5	87.6	75.7	77.9	...	78.5	...	...	71.6	
6142.490	14.0	5.62	−1.48	IK01	21.2	22.5	...	23.5	...	22.5	21.3	23.2	23.8	22.8	18.8	20.6	14.0	
6145.020	14.0	5.61	−1.37	RC02	29.7	31.9	...	31.8	35.6	31.2	30.7	28.4	29.7	32.3	29.4	30.8	...	
6155.134	14.0	5.62	−0.76	RC02	57.0	60.3	54.7	60.2	69.2	63.0	57.7	57.2	61.5	61.0	56.9	55.3	42.1	
6721.840	14.0	5.86	−0.94	RC02	29.6	35.8	34.2	34.2	38.3	35.4	31.5	27.3	31.7	35.8	43.6	42.1	20.6	
5581.980	20.0	2.52	−0.56	LUCK	...	122.8	...	...	...	123.3	...	...	121.0	...	...	...	...	
6166.440	20.0	2.52	−1.14	RT03	122.6	98.9	...	110.8	95.6	101.6	120.8	103.7	98.8	109.8	...	...	111.5	
6455.600	20.0	2.52	−1.29	IK01	107.1	88.1	112.5	100.3	79.1	88.0	104.8	87.4	84.5	93.1	117.9	114.0	98.8	
6499.650	20.0	2.52	−0.82	IK01	...	120.6	...	...	122.4	119.8	...	123.0	117.8	...	...	...	...	
5526.820	21.1	1.77	0.13	PN00	113.9	103.7	114.9	109.8	...	98.1	111.6	109.3	102.7	109.0	118.1	112.5	119.8	
6604.599	21.1	1.36	−1.48	PN00	81.3	72.2	88.0	78.4	82.9	71.6	81.9	71.1	69.2	77.4	90.8	87.4	87.1	
5648.567	22.0	2.49	−0.25	RC02	61.6	38.2	66.8	49.6	29.2	36.4	61.1	41.8	36.3	44.2	73.5	71.9	51.6	
5689.490	22.0	2.30	−0.47	RC02	...	43.0	...	...	...	45.9	...	48.2	42.1	53.3	...	...	57.1	
5716.460	22.0	2.30	−0.70	RC02	46.7	27.7	53.8	38.1	19.8	26.6	47.6	29.5	26.7	32.6	64.8	60.6	38.0	
5720.480	22.0	2.29	−0.90	RC02	38.2	21.9	45.0	30.6	15.7	22.4	38.3	24.8	26.3	25.5	55.2	52.1	31.5	
5739.464	22.0	2.25	−0.60	RC02	54.4	32.4	64.1	45.1	25.2	31.9	56.8	37.1	31.9	38.5	...	...	47.1	
5739.982	22.0	2.24	−0.67	RC02	47.1	28.5	54.0	40.1	24.9	26.2	41.7	30.2	26.0	34.0	64.5	62.5	35.0	
5903.317	22.0	1.07	−2.14	RC02	91.5	52.3	106.9	72.3	46.7	50.0	89.0	57.2	49.4	61.0	112.5	109.9	87.0	
5937.811	22.0	1.07	−1.89	RC02	101.9	62.1	120.4	81.2	55.0	60.8	102.9	65.8	60.4	70.6	...	...	95.5	
5941.752	22.0	1.05	−1.52	RC02	...	92.5	...	115.4	95.8	90.3	...	100.4	81.0	103.8	...	...	...	
5978.540	22.0	1.87	−0.50	IK01	...	...	...	...	80.1	...	112.8	88.3	80.1	...	...	...	103.6	
5999.680	22.0	2.17	−0.73	RC02	53.6	30.3	61.3	43.5	22.1	30.3	55.1	34.5	29.8	36.8	...	...	...	
6091.174	22.0	2.27	−0.42	RC02	80.5	54.0	92.0	67.6	44.6	54.1	79.7	58.7	51.5	59.5	99.0	97.8	70.3	
6126.220	22.0	1.07	−1.42	IK01	...	102.9	...	124.5	106.6	102.1	...	112.2	102.4	113.5	...	...	...	
6146.220	22.0	1.87	−1.47	RC02	...	...	...	...	...	22.8	46.5	26.5	...	...	...	70.2	...	
6186.150	22.0	2.17	−1.15	RC02	...	21.0	...	29.7	17.6	20.0	...	20.2	16.6	25.3	...	...	26.0	
6312.240	22.0	1.46	−1.55	IK01	88.9	54.0	112.0	70.6	44.4	50.7	87.9	58.4	50.4	62.7	118.1	115.8	94.3	
6497.690	22.0	1.44	−1.93	RC02	63.1	30.7	80.8	45.9	...	31.2	64.5	33.9	29.5	40.7	95.0	...	54.5	
6508.140	22.0	1.43	−1.98	RC02	57.5	26.6	82.3	41.8	19.0	23.1	61.1	29.2	23.9	34.5	107.1	...	47.8	
6554.224	22.0	1.44	−1.22	RC02	118.5	77.6	...	100.1	...	77.4	118.6	83.5	74.7	88.8	...	...	112.9	
6716.680	22.0	2.49	−1.04	RC02	19.3	...	29.2	15.3	...	9.1	22.5	10.8	...	11.6	39.4	38.1	14.1	
6743.124	22.0	0.90	−1.63	RC02	...	100.0	...	123.8	96.0	97.0	...	...	96.3	110.4	...	...	...	
6090.218	23.0	1.08	−0.06	RT03	...	100.2	...	120.1	102.2	...	...	106.0	...	110.1	...	...	...	
6216.362	23.0	0.28	−1.29	PN00	...	122.8	...	...	110.2	119.7	...	...	117.4	...	...	...	...	
6251.818	23.0	0.29	−1.34	PN00	...	109.9	...	...	98.8	108.7	...	117.1	105.2	124.7	...	...	...	
6504.160	23.0	1.18	−1.23	PN00	59.4	33.2	71.5	45.7	28.3	31.5	59.0	33.5	30.0	39.0	87.0	82.8	47.1	
5783.090	24.0	3.32	−0.50	CM05	47.1	...	48.2	41.0	19.9	28.9	45.4	35.9	31.4	36.3	54.3	51.6	40.1	
5783.890	24.0	3.32	−0.29	CM05	73.8	55.8	75.4	67.2	46.5	53.7	72.4	58.9	56.6	57.1	78.0	77.5	63.1	
5787.960	24.0	3.32	−0.08	CM05	69.3	52.8	71.1	62.2	44.3	53.0	68.1	55.7	51.1	56.5	...	...	60.3	
5537.742	25.0	2.19	−2.02	PN00	106.3	66.7	...	80.9	60.0	64.9	105.6	72.5	...	80.1	...	...	89.4	
6013.527	25.0	3.07	−0.25	PN00	...	101.5	...	117.7	93.5	100.2	...	100.3	97.8	110.9	...	...	123.4	
6016.667	25.0	3.08	−0.22	PN00	...	104.1	...	116.0	103.2	102.7	123.9	107.6	102.1	110.5	...	...	116.1	
6021.800	25.0	3.07	0.03	PN00	124.6	107.5	...	117.8	114.6	106.3	123.5	109.5	103.0	113.9	...	...	121.9	
5530.791	27.0	1.71	−2.06	PN00	92.1	70.3	104.6	82.2	79.7	65.7	91.5	73.3	67.4	76.7	103.4	103.0	90.0	
6455.034	27.0	3.63	−0.25	PN00	27.8	21.8	32.1	26.7	26.0	22.5	30.4	21.9	21.4	24.3	30.5	27.8	22.9	
6632.447	27.0	2.28	−2.00	PN00	46.7	32.9	54.7	42.8	36.8	31.9	47.6	34.2	30.7	39.1	55.4	52.2	37.9	
5578.730	28.0	1.68	−2.64	KB95	...	104.6	...	117.0	...	107.1	...	...	106.6	...	...	...	...	
6007.310	28.0	1.68	−3.34	RC02	...	...	...	...	...	65.1	...	67.0	63.8	70.1	...	...	81.5	
6086.282	28.0	4.26	−0.52	RC02	35.6	33.6	37.8	36.1	35.5	32.2	35.1	32.4	30.8	34.2	...	34.1	32.7	

Table 2—Continued

Wavelength (Å)	Species	χ (eV)	log gf	Source gf	M4 L1411	M4 L1501	M4 L1514	M4 L2307	M4 L2406	M4 L2617	M4 L3209	M4 L3413	M4 L3624	M4 L4511	M4 L4611	M4 L4613	M5 IV-81	M
6108.120	28.0	1.68	−2.45	KB95	...	114.5	...	...	...	115.2	...	119.2	114.3	121.2	...	...	...	
6175.370	28.0	4.09	−0.53	RC02	43.7	41.2	...	44.2	44.5	41.3	46.6	42.4	40.2	44.2	...	...	36.3	
6186.711	28.0	4.10	−0.97	RC02	...	20.0	...	27.6	23.7	23.4	34.3	25.1	25.9	26.4	...	...	21.4	
6204.604	28.0	4.09	−1.14	RC02	20.5	20.1	30.7	23.2	21.6	21.2	24.9	...	20.0	22.6	...	...	17.3	
6223.990	28.0	4.10	−0.99	IK01	...	22.1	...	23.9	22.2	21.7	28.1	...	21.5	21.0	...	...	17.5	
6635.122	28.0	4.42	−0.83	RC02	16.5	16.0	12.8	19.2	17.6	18.8	19.3	14.8	16.0	20.0	25.3	21.7	11.4	
5782.127	29.0	1.64	−1.72	CS02	synth	synth	synth	synth	synth	synth	synth	synth	synth	synth	synth	synth	synth	
4722.153	30.0	4.03	−0.34	KB95	...	synth	synth	synth	synth	synth	synth	synth	synth	synth	synth	synth	synth	
7070.100	38.0	1.85	−0.09	LUCK	16.7	11.5	28.9	14.0	10.2	...	15.5	...	14.4	11.1	...	...	9.6	
5570.440	42.0	1.34	0.15	SS00	61.7	36.8	70.9	52.4	32.2	...	61.2	39.3	32.5	44.8	81.4	79.5	46.4	
5274.240	58.1	1.04	−0.32	LUCK	49.0	37.0	40.5	42.2	44.8	...	43.9	38.8	36.7	41.0	49.7	50.3	30.0	
5472.300	58.1	1.24	−0.18	LUCK	31.0	20.4	33.1	24.3	21.5	...	27.8	21.4	22.3	22.4	44.2	50.0	18.2	
5322.760	59.1	0.48	−0.07	ND03	57.5	42.2	53.3	44.0	...	34.1	52.2	40.9	...	38.0	62.6	65.4	52.3	
4567.610	60.1	0.20	−1.31	DL03	43.7	26.8	40.7	33.6	28.1	24.3	33.5	29.6	25.3	28.7	51.3	56.2	41.4	
4706.540	60.1	0.00	−0.71	DL03	...	77.5	109.0	94.2	100.1	76.2	...	84.4	79.7	86.7	117.8	120.1	101.4	
4859.030	60.1	0.32	−0.44	DL03	95.3	64.0	100.5	83.6	78.3	62.7	85.7	...	91.1	69.1	109.7	98.3	...	
4902.040	60.1	0.06	−1.34	DL03	80.2	...	...	...	...	...	...	57.5	...	62.8	...	...	75.0	
5092.790	60.1	0.38	−0.61	DL03	...	58.5	...	...	64.3	...	...	...	...	...	...	...	74.4	
5249.580	60.1	0.98	0.20	DL03	83.8	65.9	84.8	75.9	...	...	81.5	72.4	62.5	69.5	91.9	88.7	80.4	
5306.460	60.1	0.86	−0.97	DL03	...	16.5	36.6	22.7	17.2	...	32.4	17.9	14.3	14.4	...	...	24.0	
5311.450	60.1	0.99	−0.42	DL03	63.3	36.7	64.7	47.8	40.0	...	60.2	39.3	34.0	43.9	...	...	40.3	
5485.700	60.1	1.26	−0.12	DL03	43.1	29.2	...	34.6	28.7	...	44.8	32.4	...	31.5	...	...	33.3	
5740.860	60.1	1.16	−0.53	DL03	28.5	19.9	...	...	...	...	27.1	20.5	17.6	22.6	35.4	...	19.0	
5811.570	60.1	0.86	−0.86	DL03	28.9	18.2	29.4	23.5	16.8	...	27.0	20.3	19.3	18.2	39.7	40.8	24.5	
4536.510	62.1	0.10	−1.28	LD06	53.7	36.5	...	45.1	...	...	51.9	39.9	35.8	39.9	...	...	...	
4577.690	62.1	0.25	−0.65	LD06	synth	synth	synth	synth	synth	synth	synth	synth	synth	synth	synth	synth	synth	
4642.230	62.1	0.38	−0.46	LD06	69.0	...	...	60.2	62.1	52.1	63.4	57.0	48.8	55.8	72.4	77.3	72.4	
4676.900	62.1	0.04	−0.87	LD06	68.6	55.1	74.8	65.7	64.6	53.9	59.9	60.1	53.9	59.9	83.5	82.7	82.9	
4316.050	64.1	0.66	−0.45	DL06	synth	synth	synth	synth	synth	synth	synth	synth	synth	synth	synth	synth	synth	
4483.330	64.1	1.06	−0.42	DL06	synth	synth	synth	synth	synth	synth	synth	synth	synth	synth	synth	synth	synth	
4093.155	72.1	0.05	−1.15	LH07	synth	synth	synth	...	synth	synth	synth	synth	...	synth	synth	...	synth	
5989.045	90.1	0.19	−1.41	NZ02	synth	synth	synth	synth	synth	synth	synth	synth	synth	synth	synth	synth	synth	

References. — CM05 = Cohen & Meléndez (2005); CS02 = (Cunha et al. 2002); DL03 = Den Hartog et al. (2003); DL06 = Den Hartog et al. (2006); IK01 = Ivans et al. (1999); KB95 = Kurucz & Bell (1995); LD06 = Lawler et al. (2006
Lawler et al. (2007); LUCK = R. E. Luck (priv. comm.); ND95 = Norris et al. (1995); NZ02 = Nilsson et al. (2002); PN00 = Prochaska et al. (2000); RC02 = Ramírez & Cohen (2002); RT03 = Reddy et al. (2003); SS00 = Smith et al. (2000)

Table 3. Adopted solar abundances.

Species	$\log \epsilon(\mathrm{X})$	Source
Si	7.55	1
Ca	6.31	2
Sc	3.05	2
Ti	4.90	2
V	4.00	2
Cr	5.64	2
Mn	5.39	2
Fe	7.50	1
Co	4.92	2
Ni	6.23	2
Cu	4.21	1
Zn	4.60	1
Sr	2.92	1
Mo	1.92	1
Ce	1.58	1
Pr	0.58	3
Nd	1.45	3
Sm	1.00	3
Gd	1.11	3
Hf	0.88	3
Th	0.06	3

References. — 1 = Grevesse & Sauval (1998); 2 = Asplund et al. (2005); 3 = Grevesse et al. (2007)

Table 4. Abundance ratios [X/Fe] for Ca to Zn.

Star	[Si/Fe]	[Ca/Fe]	[Sc/Fe]	[Ti/Fe]	[V/Fe]	[Cr/Fe]	[Mn/Fe]	[Co/Fe]	[Ni/Fe]	[Cu/Fe]	[Zn/Fe]
M4 L1411	0.58	0.43	0.17	0.42	0.18	0.11	−0.16	0.04	0.10	−0.27	...
M4 L1501	0.64	0.45	0.21	0.35	0.18	0.07	−0.23	0.01	0.15	−0.27	0.24
M4 L1514	0.51	0.34	0.00	0.44	0.15	0.06	...	0.00	0.09	−0.33	0.27
M4 L2307	0.54	0.47	0.17	0.39	0.17	0.09	−0.23	0.01	0.14	−0.31	0.19
M4 L2406	0.46	0.19	0.04	0.16	0.04	−0.12	−0.36	−0.03	0.06	−0.25	0.30
M4 L2617	0.61	0.44	0.04	0.38	0.23	0.05	−0.23	0.01	0.10	−0.31	0.15
M4 L3209	0.60	0.44	0.02	0.50	0.28	0.14	−0.15	0.07	0.17	−0.2	0.15
M4 L3413	0.44	0.42	0.13	0.41	0.20	0.11	−0.24	0.01	0.05	−0.22	0.13
M4 L3624	0.62	0.47	0.15	0.38	0.21	0.11	−0.25	0.03	0.14	−0.22	0.19
M4 L4511	0.68	0.43	0.17	0.33	0.15	0.05	−0.24	0.01	0.10	−0.23	0.17
M4 L4611	0.70	0.50	0.20	0.59	0.25	0.13	...	−0.13	0.17	−0.46	0.29
M4 L4613	0.52	0.42	0.10	0.55	0.25	0.16	...	−0.03	0.14	−0.31	0.20
M5 IV-81	0.32	0.37	0.08	0.40	0.11	0.08	−0.24	−0.08	−0.02	−0.52	−0.07
M5 IV-82	0.32	0.37	0.19	0.33	0.19	0.21	−0.32	−0.05	−0.01	−0.52	−0.02

Table 5. Abundance ratios [X/Fe] for Sr to Th.

Star	[Sr/Fe]	[Mo/Fe]	[Ce/Fe]	[Pr/Fe]	[Nd/Fe]	[Sm/Fe]	[Gd/Fe]	[Hf/Fe]	[Th/Fe]
M4 L1411	0.67	0.18	0.61	0.62	0.64	0.47	0.42	0.43	0.49
M4 L1501	0.74	0.13	0.52	0.56	0.43	0.47	0.36	0.39	0.60
M4 L1514	0.87	0.16	0.36	0.33	0.45	0.32	0.14	0.37	0.33
M4 L2307	0.67	0.20	0.51	0.45	0.51	0.52	0.27	...	0.50
M4 L2406	0.69	−0.02	0.27	...	0.11	0.27	0.08	0.30	0.36
M4 L2617	...	...	...	0.43	0.31	0.43	0.33	0.40	0.66
M4 L3209	0.71	0.24	0.52	0.51	0.50	0.41	0.35	0.40	0.51
M4 L3413	...	0.17	0.52	0.50	0.50	0.44	0.35	0.33	0.59
M4 L3624	0.91	0.13	0.56	...	0.44	0.41	0.31	...	0.70
M4 L4511	0.61	0.13	0.53	0.41	0.42	0.43	0.33	0.37	0.53
M4 L4611	...	0.36	0.48	0.44	0.35	0.66	0.21	0.39	0.35
M4 L4613	...	0.31	0.65	0.57	0.58	0.54	0.33	...	0.41
M5 IV-81	0.51	0.02	0.14	0.40	0.32	0.41	0.59	0.28	0.64
M5 IV-82	...	−0.17	0.26	0.37	0.31	0.50	0.45	0.23	0.59

Table 6. Abundance Dependences on Model Parameters for M4 L2307.

Species	$T_{\rm eff}$+50	log g+0.2	ξ_t+0.2	Total[a]
[Si/Fe]	0.01	−0.03	0.02	0.04
[Ca/Fe]	0.10	−0.09	−0.04	0.14
[Sc/Fe]	0.02	0.01	−0.08	0.09
[Ti/Fe]	0.12	−0.08	0.01	0.14
[V/Fe]	0.13	−0.07	−0.01	0.15
[Cr/Fe]	0.09	−0.09	0.01	0.13
[Mn/Fe]	0.08	−0.08	−0.08	0.13
[Fe/H]	−0.01	0.04	−0.03	0.05
[Co/Fe]	0.05	−0.04	0.01	0.06
[Ni/Fe]	0.03	−0.04	0.01	0.05
[Cu/Fe][b]	0.06	−0.04	−0.05	0.09
[Zn/Fe][b]	−0.01	−0.02	−0.04	0.05
[Sr/Fe]	0.10	−0.09	0.05	0.15
[Mo/Fe]	0.12	−0.08	0.01	0.14
[Ce/Fe]	0.04	0.01	0.03	0.05
[Pr/Fe]	0.04	−0.01	0.03	0.04
[Nd/Fe]	0.05	−0.01	−0.02	0.05
[Sm/Fe][b]	0.04	−0.02	−0.02	0.04
[Gd/Fe][b]	0.03	−0.01	0.03	0.05
[Hf/Fe][c]	0.03	−0.01	0.03	0.04
[Th/Fe][b]	0.05	0.01	0.04	0.06

[a]The total value is the quadrature sum of the three individual abundance dependences

[b]For elements whose abundances were derived via synthetic spectra, we assumed an equivalent width that produced the final abundance

[c]Since no abundance was derived for Hf, we assumed an equivalent width that produced the mean cluster abundance

Table 7. Mg isotope ratios.

Star	^{24}Mg:^{25}Mg:^{26}Mg
M4 L1411	80:10:10
M4 L1501	...
M4 L1514	80:10:10
M4 L2307	72:14:14
M4 L2406	...
M4 L2617	74:13:13
M4 L3209	74:13:13
M4 L3413	80:10:10
M4 L3624	78:11:11
M4 L4511	80:10:10
M4 L4611	80:10:10
M4 L4613	78:11:11
M5 IV-81	80:10:10
M5 IV-82	78:11:11

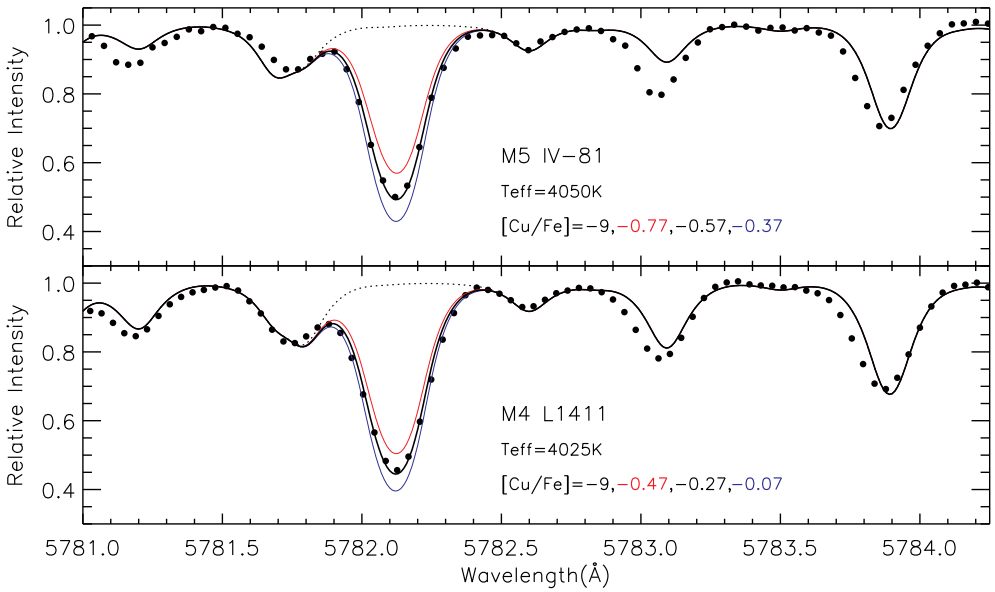

Fig. 1.— Observed spectra (filled circles) and synthetic spectra (solid and dotted lines) for M5 IV-81 (upper) and M4 L1411 (lower) near the 5782Å Cu I line. The synthetic spectra show the best fit (thick black line), unsatisfactory fits ± 0.2 dex (thin red and blue lines), and a fit with no Cu (dotted line).

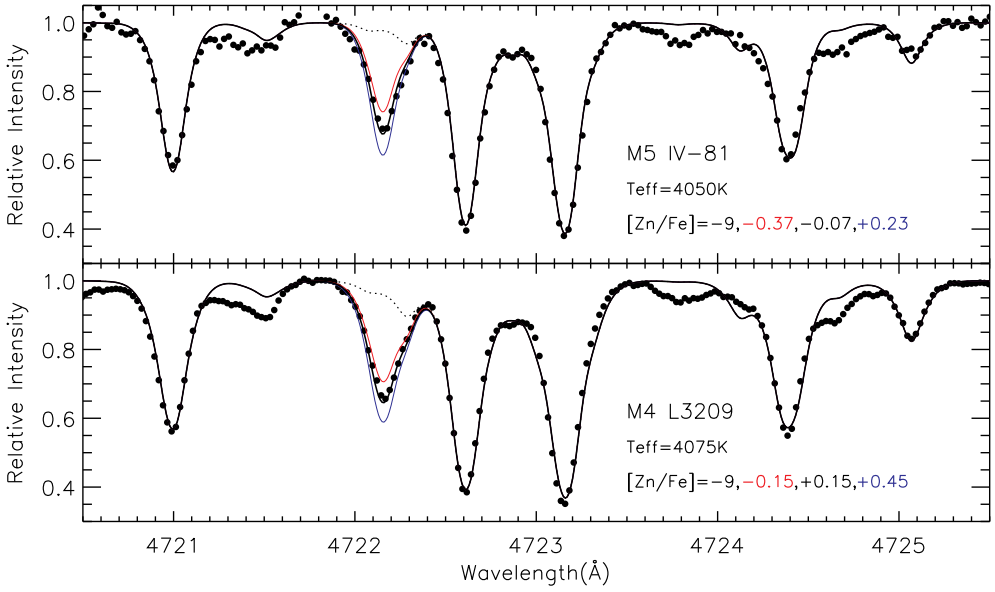

Fig. 2.— Same as Figure 1 but for the 4722Å Zn I line in stars M5 IV-81 and M4 L3209 (unsatisfactory fits ± 0.3 dex are shown).

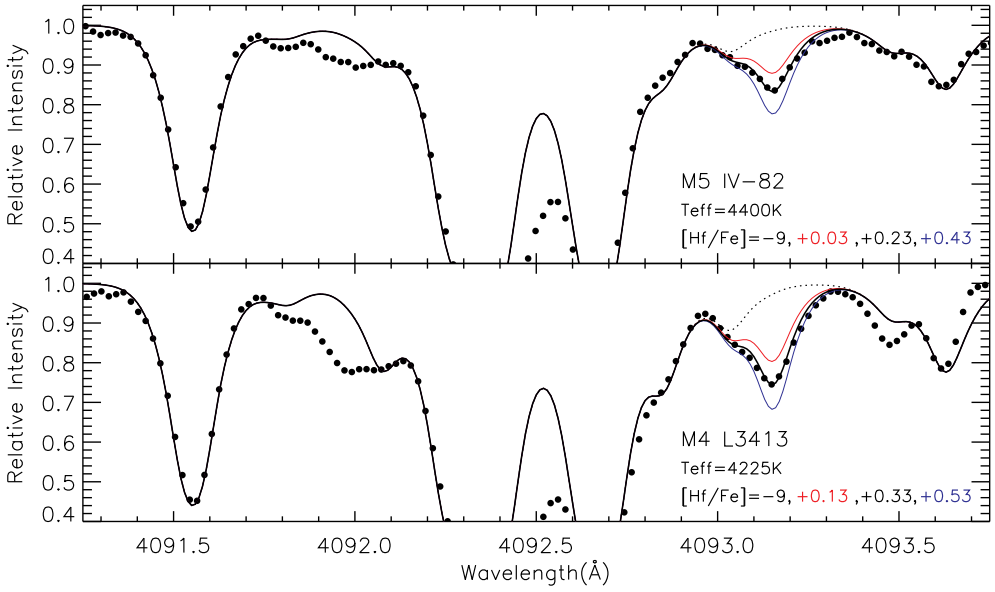

Fig. 3.— Same as Figure 1 but for the 4093Å Hf II line in stars M5 IV-82 and M4 L3413 (unsatisfactory fits ± 0.2 dex are shown).

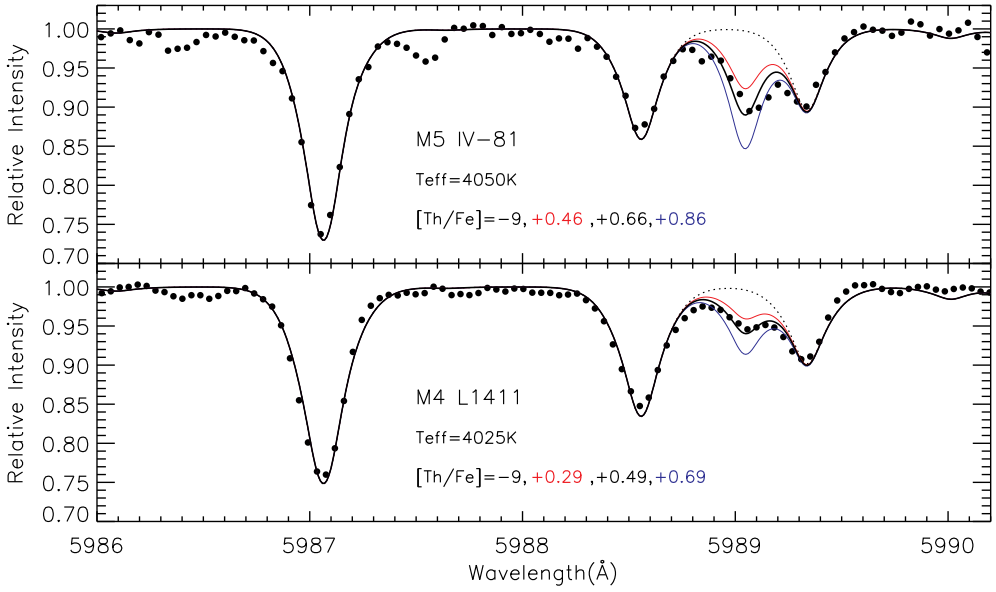

Fig. 4.— Same as Figure 1 but for the 5989Å Th II line (unsatisfactory fits ± 0.2 dex are shown).

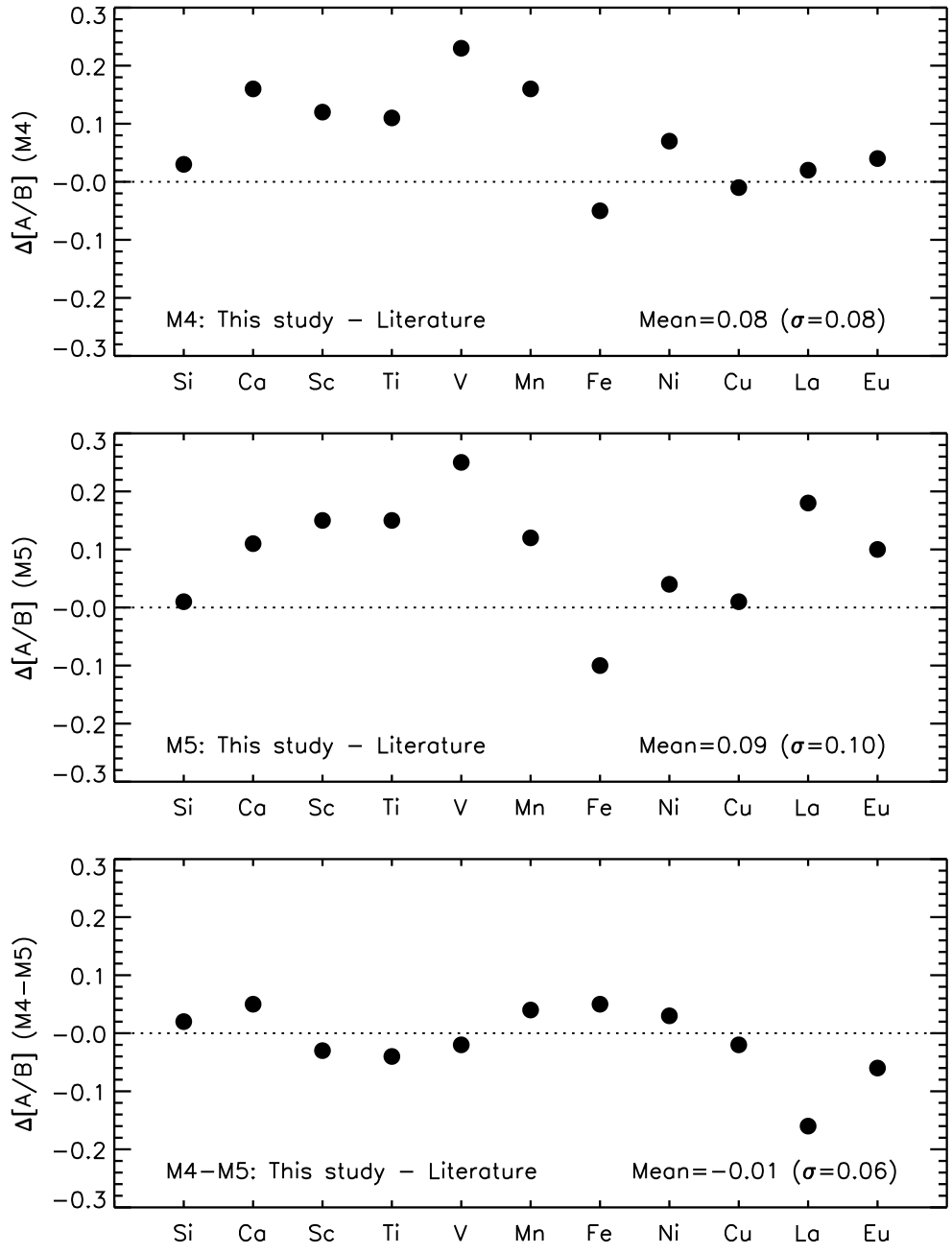

Fig. 5.— A comparison of the mean cluster values [X/Fe] and [Fe/H] between this study and the literature for M4 (upper), M5 (middle), and M4−M5 (lower). Literature values are from Ivans et al. (1999, 2001) except Mn (Sobeck et al. 2006) and Cu (Simmerer et al. 2003). The mean differences and standard deviations are shown.

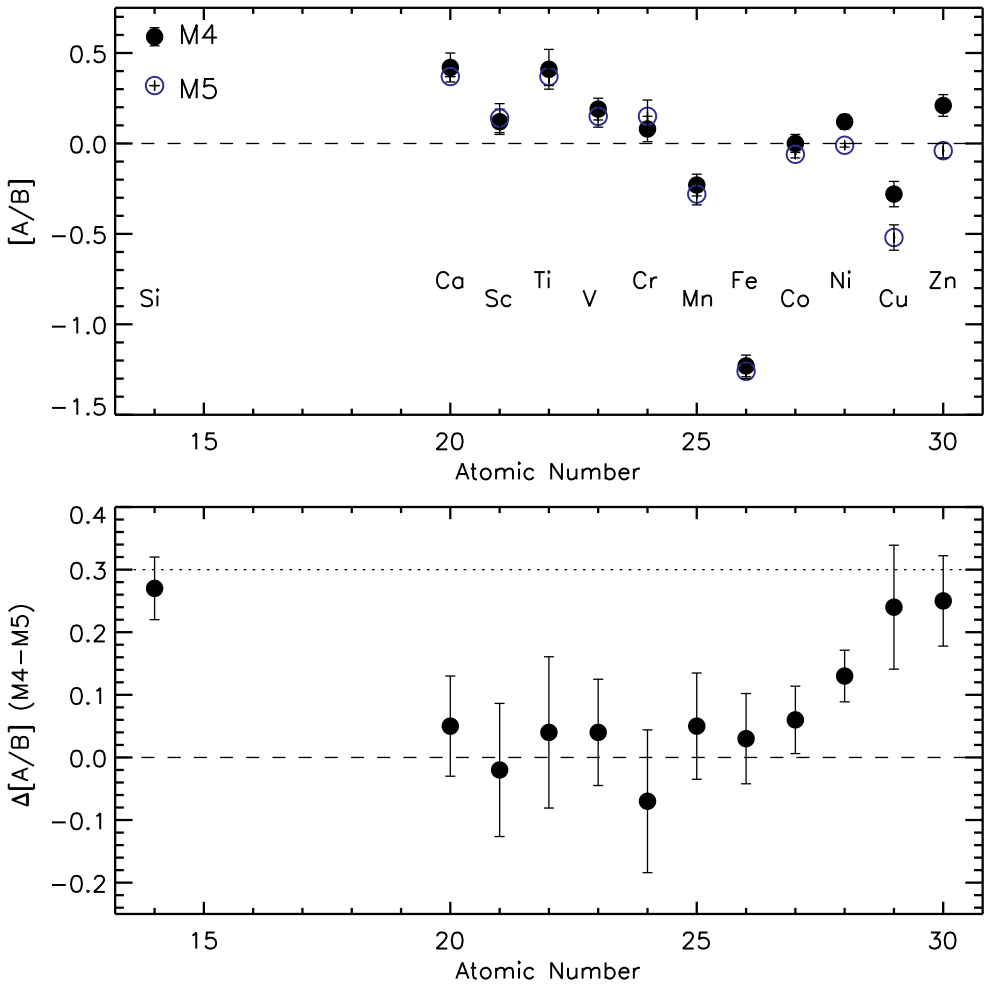

Fig. 6.— The upper panel shows [X/Fe] for the elements Si to Zn as well as [Fe/H] for M4 (filled circles) and M5 (open blue circles). The lower panel shows the difference in abundance ratios, Δ[X/Fe] (M4−M5).

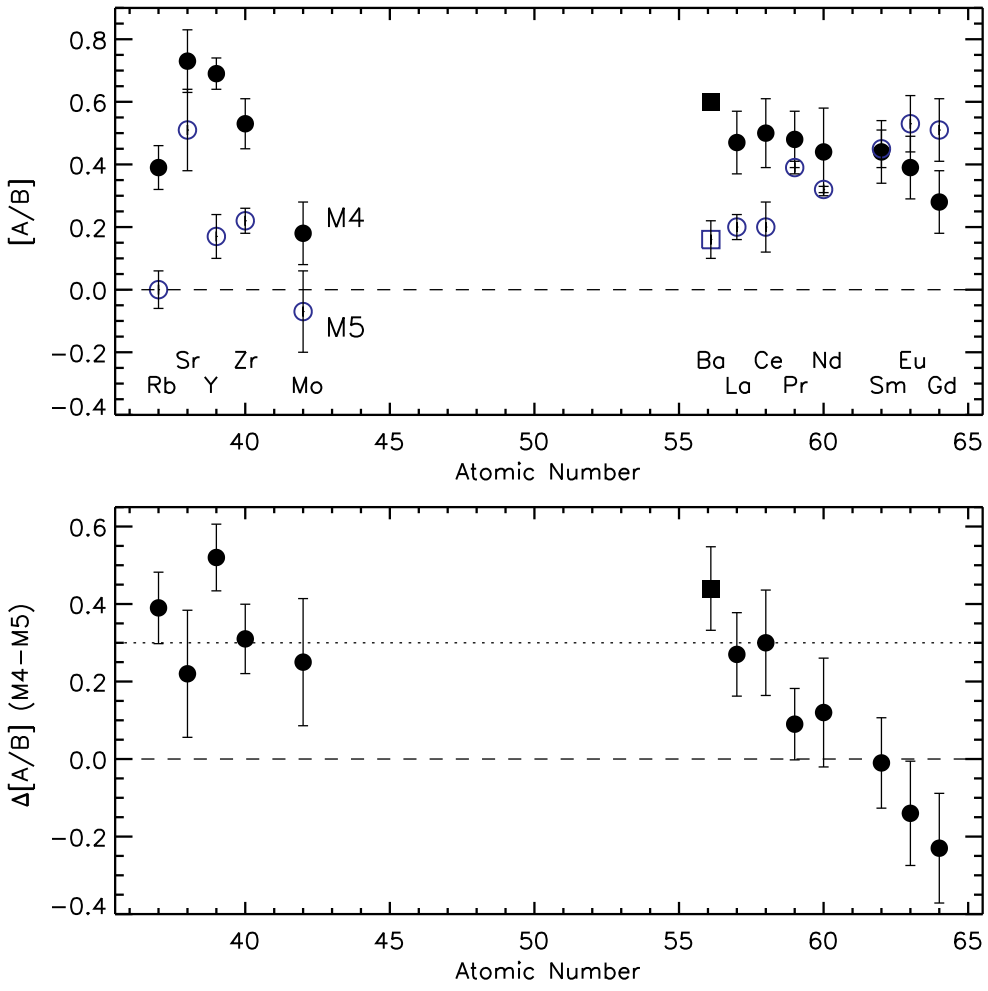

Fig. 7.— The same as Figure 6 but for the elements Rb to Gd. All data points are from this study and Yong et al. (2008), except Ba which is taken from Ivans et al. (1999, 2001).

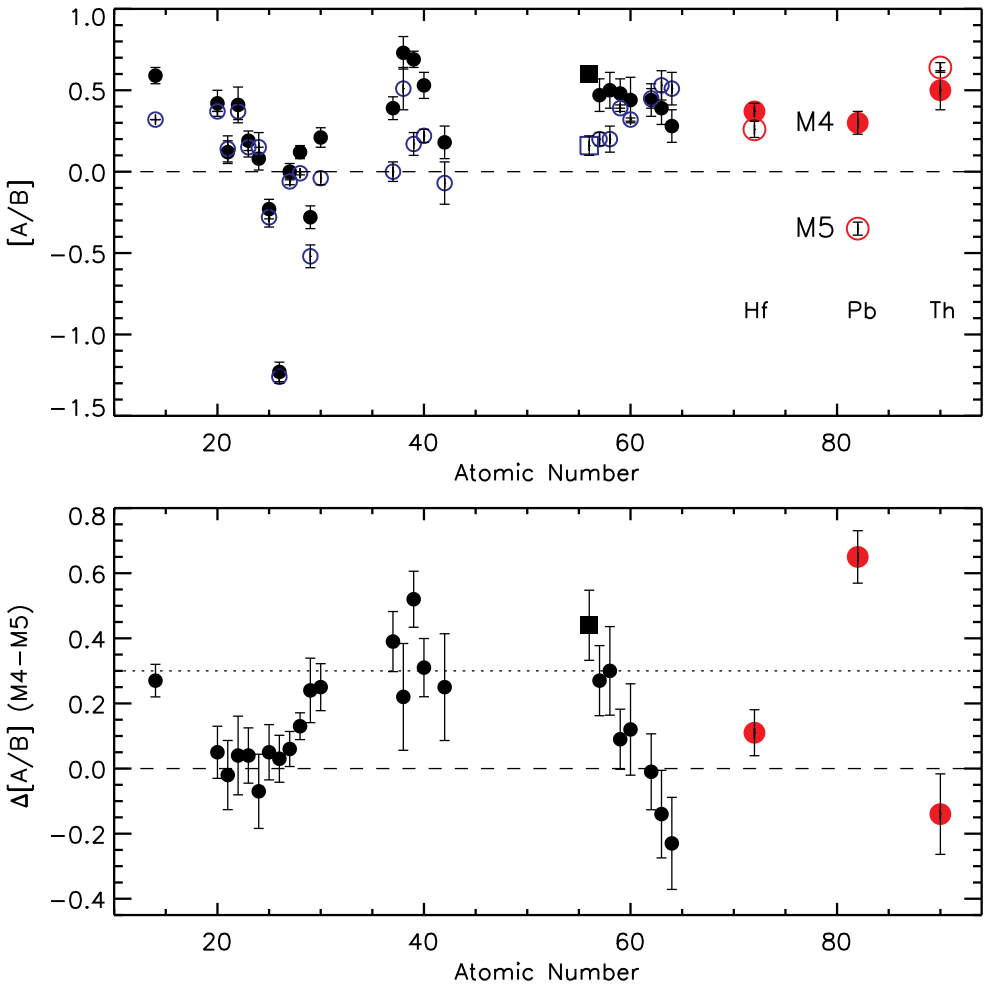

Fig. 8.— The same as Figures 6 and 7 but for all elements. The heavy neutron-capture elements Hf, Pb, and Th are highlighted in red.

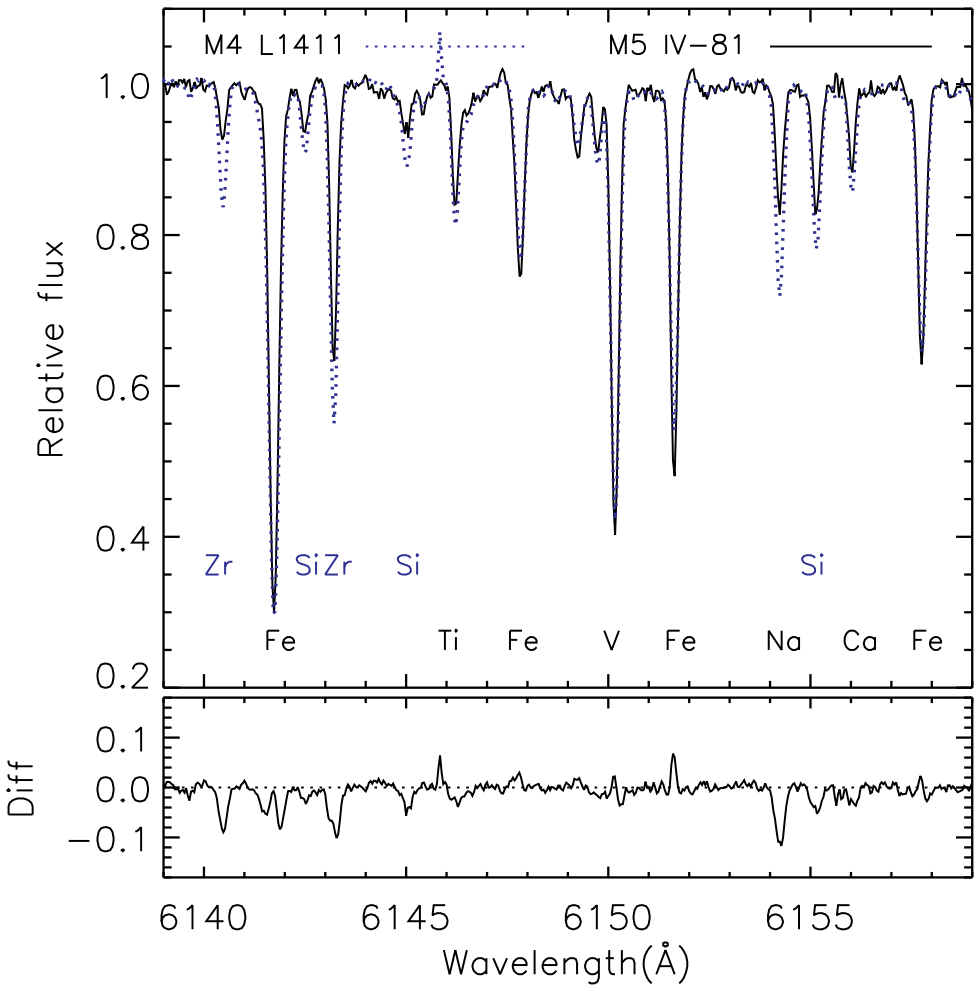

Fig. 9.— The upper panel shows observed spectra for M4 L1411 (dotted blue line) and M5 IV-81 (solid black line). Various lines within the wavelength region are identified. The lower panel shows the difference, M4 L1411 − M5 IV-81 after interpolating and rebinning the spectra.

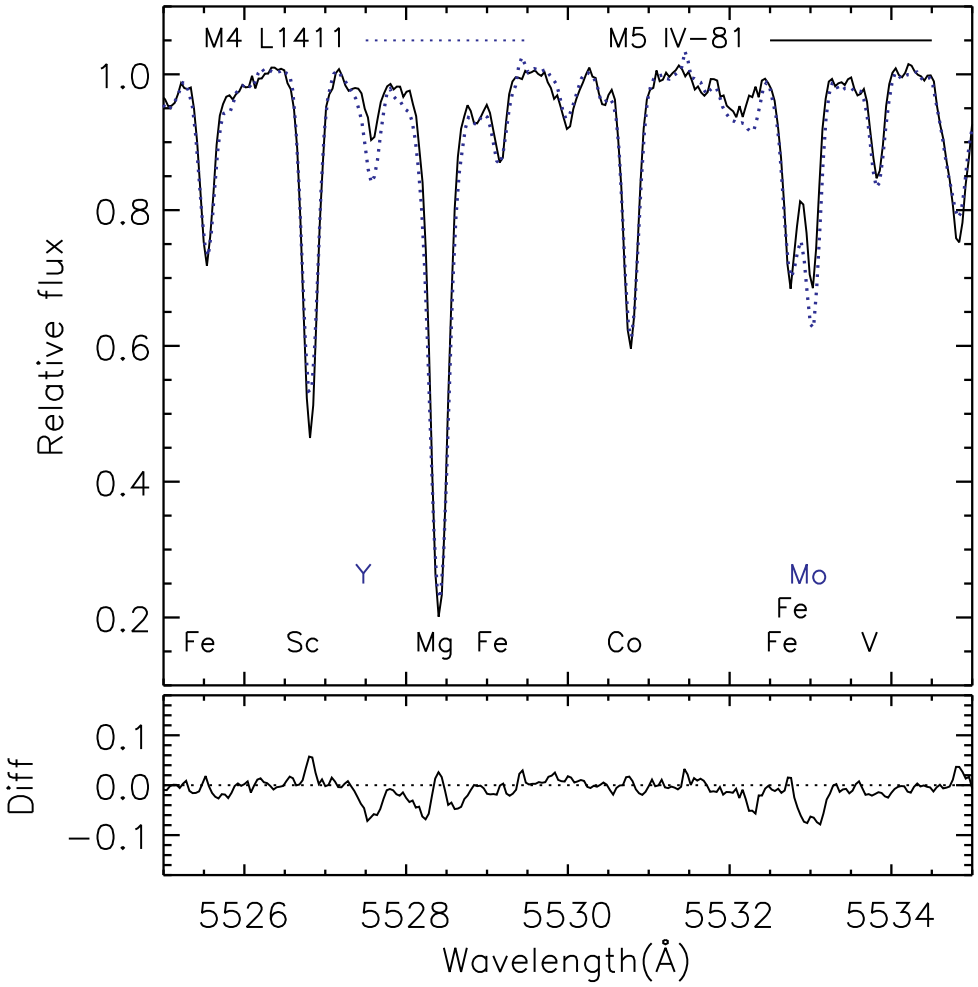

Fig. 10.— Same as Figure 9 but for a different wavelength region.

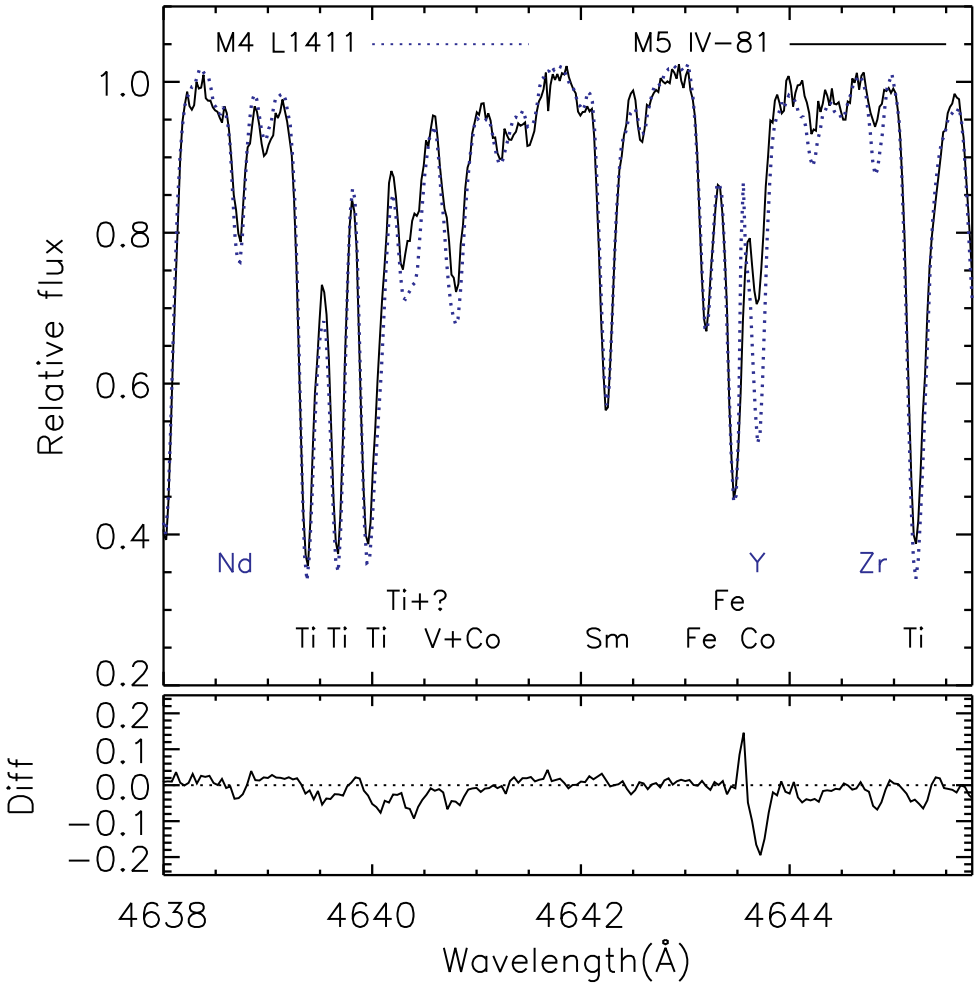

Fig. 11.— Same as Figure 9 but for a different wavelength region.

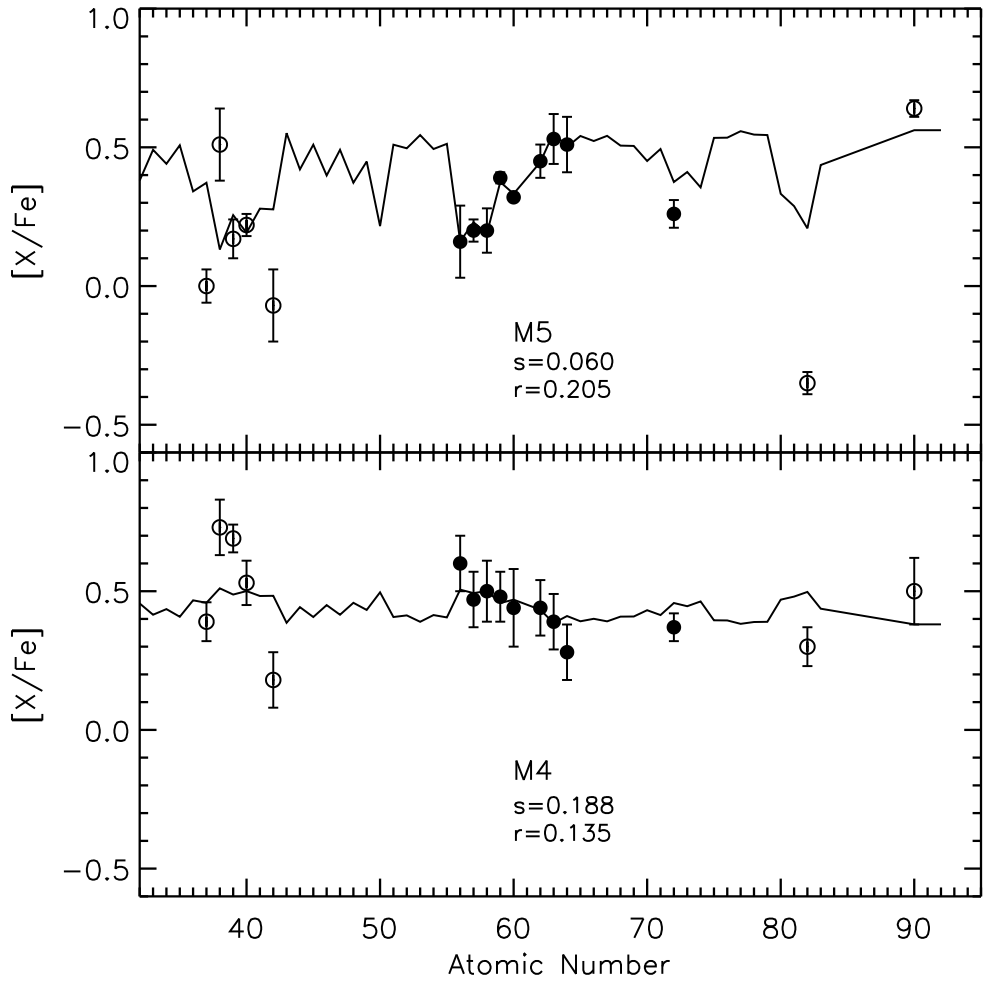

Fig. 12.— Abundance ratios [X/Fe] for Rb to Th in M5 (upper) and M4 (lower). In both panels, we show the best fit predictions to the elements from Ba to Hf (filled circles) using scaling factors s and r which were multiplied by the solar *s*-process and *r*-process abundances respectively.

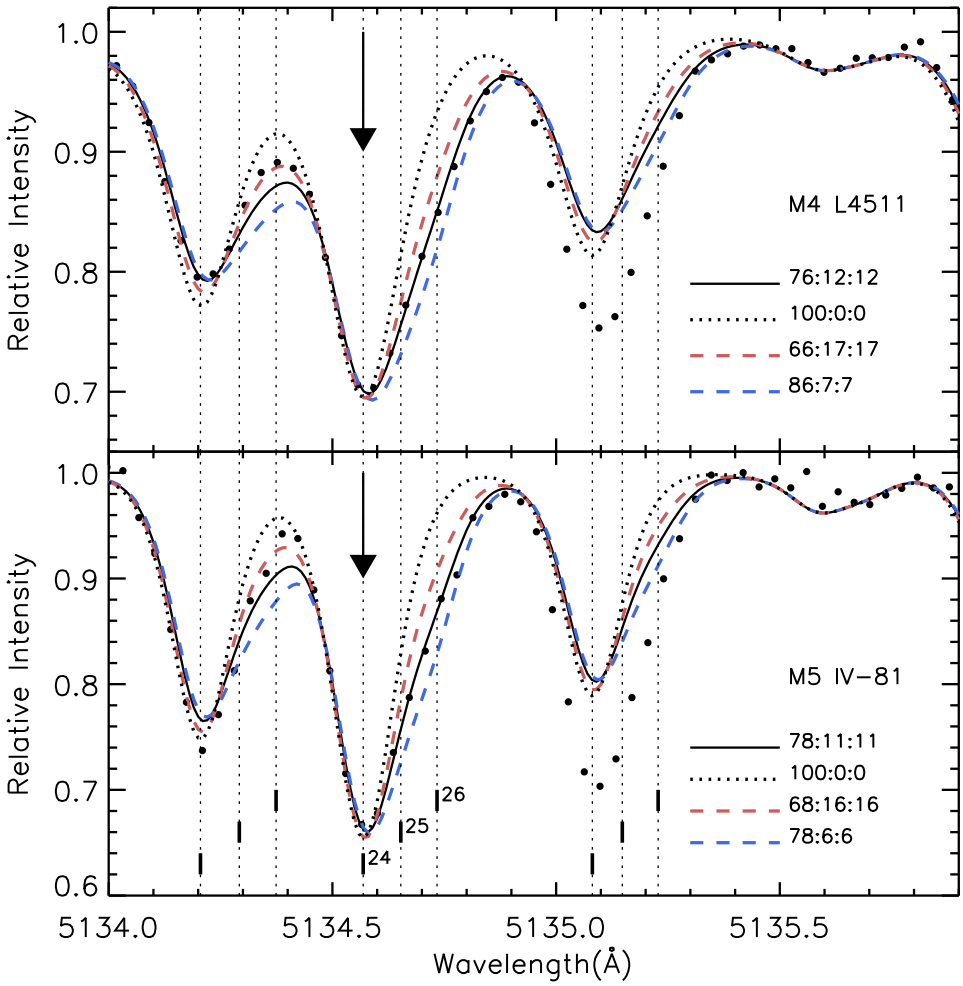

Fig. 13.— Spectra of M4 L4511 (upper) and M5 IV-81 near the 5134.6Å MgH line. The positions of ^{24}MgH, ^{25}MgH, and ^{26}MgH are marked by dashed lines. The filled circles represent the observed spectra, the best fit is shown by the solid line, and unsatisfactory ratios are also shown.